Quaternary Science Reviews 269 (2021) 107137

Contents lists available at ScienceDirect

Quaternary Science Reviews

journal homepage: www.elsevier.com/locate/quascirev

# Hydroclimate variability during the last 2700 years based on stalagmite multi-proxy records in the central-western Mediterranean

Mercè Cisneros [a, *], Isabel Cacho [a], Ana Moreno [b], Heather Stoll [c], Judit Torner [a], Albert Català [a], R. Lawrence Edwards [d], Hai Cheng [e], Joan J. Fornós [f]

[a] GRC Geociències Marines, Departament de Dinàmica de la Terra i de l'Oceà, Facultat de Ciències de la Terra, Universitat de Barcelona, Barcelona, Spain
[b] Departamento de Procesos Geoambientales y Cambio Global, Instituto Pirenaico de Ecología – CSIC, Zaragoza, Spain
[c] Department of Earth Sciences, ETH Zürich, Switzerland
[d] Department of Earth and Environmental Sciences, University of Minnesota, MN, 55455, USA
[e] Institute of Global Environmental Change, Xian Jiaotong University, Xian, 710049, China
[f] Grup de Recerca en Ciències de la Terra, Universitat de les Illes Balears, Mallorca, Spain

ARTICLE INFO

*Article history:*
Received 30 July 2021
Accepted 2 August 2021
Available online 19 August 2021

Handling Editor: Mira Matthews

*Keywords:*
Stalagmites
Muti-proxy records
Hydroclimate variability
Late Holocene
Central-western Mediterranean

ABSTRACT

This study presents the first high-resolution speleothem-based hydrological reconstruction for much of the last 2.7 kyr in the central-western Mediterranean. The paleohydrological information comes from a combination of five U-Th dated stalagmites from two Mallorca island caves. Interpretations are based on high-resolution records of $\delta^{18}O$, $\delta^{13}C$ and trace element analyses combined with information from mineralogical X-ray diffraction, fabrics and morphological features, and cave monitoring data.

None of the studied stalagmites cover the whole 2.7 kyr period but they provide sufficient overlap to replicate most of the discussed climatic intervals with the exception of the Medieval Climate Anomaly (MCA), which is represented by a hiatus. Taking into account the results of five years farmed calcite collected in glass plates and cave environmental parameters, we argue that main patterns in the stalagmite geochemical records are mostly controlled by changing rates of prior calcite precipitation (PCP) that respond to hydrological changes in the region. We apply a principal component analysis to the stalagmite geochemical data set and a composite $\delta^{18}O$ record to obtain a robust regional hydrological record.

This record supports wet conditions for the early Roman Period (RP), the first half of the Early Middle Ages (EMA) and the Little Ice Age (LIA), and drier conditions for the late RP, the late EMA and the entire MCA. These results are discussed in the context of other climatic and oceanographic records from the region including paleo North Atlantic Oscillation (NAO) records. This ocean-atmosphere approach suggests complex non-stationary climate patterns for the last 2.7 kyr, including the occurrence of both wet-warm and wet-cold intervals and underlying the complex interaction of factors controlling climate evolution in the region. Overall, positive (negative) NAO phases appear coincident with drier (wetter) conditions for all the examined period at decadal time-scales.



## 1. Introduction

The Mediterranean region has been identified as a primary hotspot vulnerable to the current climate change situation (Giorgi, 2006) and expected to become warmer, and also drier during the twenty-first century (Adloff et al., 2015). This is a situation that is already confirmed by last five decades observations from the Balearic Islands, where rates of warming and precipitation reduction are even higher than those expected from the currently available climate predictions (Homar et al., 2010). But the absence of hydrological records for the last few millennia precludes the assessment of its sensitivity to recent natural climate variability.

Most paleoclimate studies of Mediterranean and Southern European have focused on pre-Holocene hydroclimate or have only partial coverage for the last 3 kyr (e.g.: Bar-Matthews et al., 2003;

* Corresponding author. GRC Geociències Marines, Departament de Dinàmica de la Terra i de l'Oceà, Facultat de Ciències de la Terra, Universitat de Barcelona, Barcelona, Spain.
*E-mail address:* mercecisnerosb@gmail.com (M. Cisneros).

https://doi.org/10.1016/j.quascirev.2021.107137

Frisia et al., 2003, 2005, 2006; McMillan et al., 2005; Mangini et al., 2005; Martín-Chivelet et al., 2011; Railsback et al., 2011; Wassenburg et al., 2013; Cheng et al., 2015; Ait Brahim et al., 2017, 2018, 2019; Budsky et al., 2019). In the context of Mallorca, speleothem studies have been based on phreatic overgrowths and reconstruction of past sea-levels (Vesica et al., 2001; Polyak et al., 2018; Dumitru et al., 2019) or paleoclimate reconstructions from periods prior to the Last Glacial Maximum (Hodge, 2004; Hodge et al., 2008; Dumitru et al., 2018; Torner et al., 2019). Therefore, Mediterranean speleothem records for the last 3 kyr are very scarce, and particularly for the western Mediterranean region. Even for Western Europe, which is the region with the highest density of published speleothem $\delta^{18}O$ records worldwide (see for example compilation by SISAL group, Lechleitner et al., 2018), this time period is poorly represented.

A recent global compilation of paleoclimatic records from last few millennia reveals a significant regional heterogeneity in climatic evolution of this period (Neukom et al., 2019) highlighting the need of complete regional climate reconstructions to assets its sensitivity to recent natural climate variability forcings. In this regard, some marine records close to the Balearic Islands have shown significant sea surface temperature (SST) changes for the last 2.7 kyr (Cisneros et al., 2016). In particular, these records indicate the Roman Period (RP) as the warmest interval, a common feature in other parts of the Mediterranean Sea (Margaritelli et al., 2020), while coldest conditions occurred during the second half of the Little Ice Age (LIA). These Balearic marine sediments have also provided an indicator of changes in deep convection in the western Gulf of Lions, an oceanographic process controlled by temperature and evaporation-precipitation conditions in the region (Cisneros et al., 2019). Episodes interpreted as strong Western Mediterranean Deep Water (WMDW) formation, occurred mostly during relatively warm intervals, which underlines the potential critical role that hydrological conditions could have exerted as main controller of this process. This hypothesis is difficult to test because of the lack of records with an unequivocal evidence of hydrological changes in the region.

This study aims to fill this gap by characterising the hydroclimate variability of the last 2700 years for the first time in the central western-Mediterranean region using five Mallorca stalagmites. For this purpose, we have integrated geochemical analysis ($\delta^{18}O$, $\delta^{13}C$ and trace element ratios) with petrological and textural tools. In addition, these data are discussed and interpreted with support of a cave monitoring exercise. Factors controlling the variability of the different applied geochemical records are statistically explored using correlation and principal component analysis (PCA). This multi-proxy strategy is used to support the interpretation of the stalagmite $\delta^{18}O$ records as a robust proxy for past hydroclimate conditions in Mallorca, which are also discussed in the context of other previous relevant paleoclimatic and paleoceanographic records of the region for the last 2.7 kyr.

## 2. Cave and climatic settings

### 2.1. Caves description

The speleothems were recovered from *Sa Balma des Quartó* cave (*Quartó* hereinafter) and *Coves del Pirata* (*Pirata* hereinafter) located in the south-east of Mallorca in the central-western Mediterranean Sea (Fig. 1). The caves were formed in very porous Upper-Miocene reef limestone (Ginés et al., 2014). The caves are found in close proximity (<1 km) and experience the same climate conditions and vegetation type. Currently, the surrounding landscape is dominated by Mediterranean vegetation (species like *Quercus ilex*, *Pistacia lentiscus* or genus *Juniperus*; Bolòs, 1996), which is relatively undisturbed by human activities.

*Quartó* cave consists of a wide spacious chamber formed by collapse, the bottom of which is 10.5 m above sea level and 12.5 m from the surface (Fig. 2a and b). The chamber has a rich decoration of speleothems, including abundant straw stalactites. Access to the cave is a small and vertical hole in the outside rock-shelter and the cave is more ventilated during the cold season. Most of the stalagmites and monitoring data here presented belong to this cave (Fig. 2a and b).

*Pirata* cave, which is part of a larger system of connected galleries, comprises numerous chambers divided by columns and stalagmite walls and has a complicated topography. Its tour-length is approximately ~800 m and consists of two main sectors (Martel et al., 1903; Ginés and Ginés, 1976; Garcia et al., 1986). One of the speleothems of this study (named Constantine) was found in the south portion of the so-called Classic Sector.

The cave environmental data used to discuss the monitoring results from Quartó cave are complemented with some data from the nearby Coves del Drac (*Drac* hereinafter). Drac cave is also located in the south-east of Mallorca (Fig. 1), formed in Upper-Miocene reef limestone and consists in two main sectors. The touristic sector has been significantly modified since 1898 (Ginés and Ginés, 2011) and is one of the most visited caves in Europe. The data used here correspond to the restricted sector that is not impacted by artificial ventilation and it has been the research focus of a number of publications (e.g.: Boop et al., 2014; Dumitru et al., 2015, 2017).

### 2.2. Climatic conditions

The Balearic Islands present a typical Mediterranean climate, characterized by mild wet winters and warm to hot, dry summers (Lionello et al., 2006). Maximum rainfall occurs during the autumn (Fig. 3a and b).

Present-day interannual climate variability, particularly precipitation intensities in the studied area are associated to the North Atlantic Oscillation (NAO) (Cassou et al., 2010; Josey et al., 2011). The NAO is defined by the difference in atmospheric pressure between Iceland low and Azores high. Positive (negative) NAO phases lead to stronger winter storms crossing the Atlantic on a more northerly track, which results in warm and wet winters in Europe and dry (wet) conditions over the Mediterranean (Hurrell et al., 1995, 2003; Trigo et al., 2002; Lionello and Sanna, 2005; Mariotti, 2011). But there are other modes of climate variability that also contribute to the interannual climate variability of the region as the East Atlantic (EA), East Atlantic/West Russian (EA/WR) and Scandinavian (SCAN) patterns, in order of significance (Cassou et al., 2010; Josey et al., 2011).

## 3. Material and methods

### 3.1. Cave monitoring

Additional data of a monitoring exercise performed in *Quartó* cave from 2013 to 2018 is also presented and discussed in order to better identify the environmental factors controlling the chemical signature of the cave carbonate. This data set consists of cave environmental parameters such as temperature and $CO_2$ concentrations, drip rates and waters, carbonate precipitation rates and chemical compositions of farmed calcite collected on glass plates at seasonal scale (stable isotopes and Mg/Ca ratios). During this period the cave was visited every three months to allow the recovery of the main seasonal signal within the farmed calcite (Table S.1). The discharge rate (drips/min) was routinely measured in five sites during each visit (Fig. 2b), additional sites were occasionally

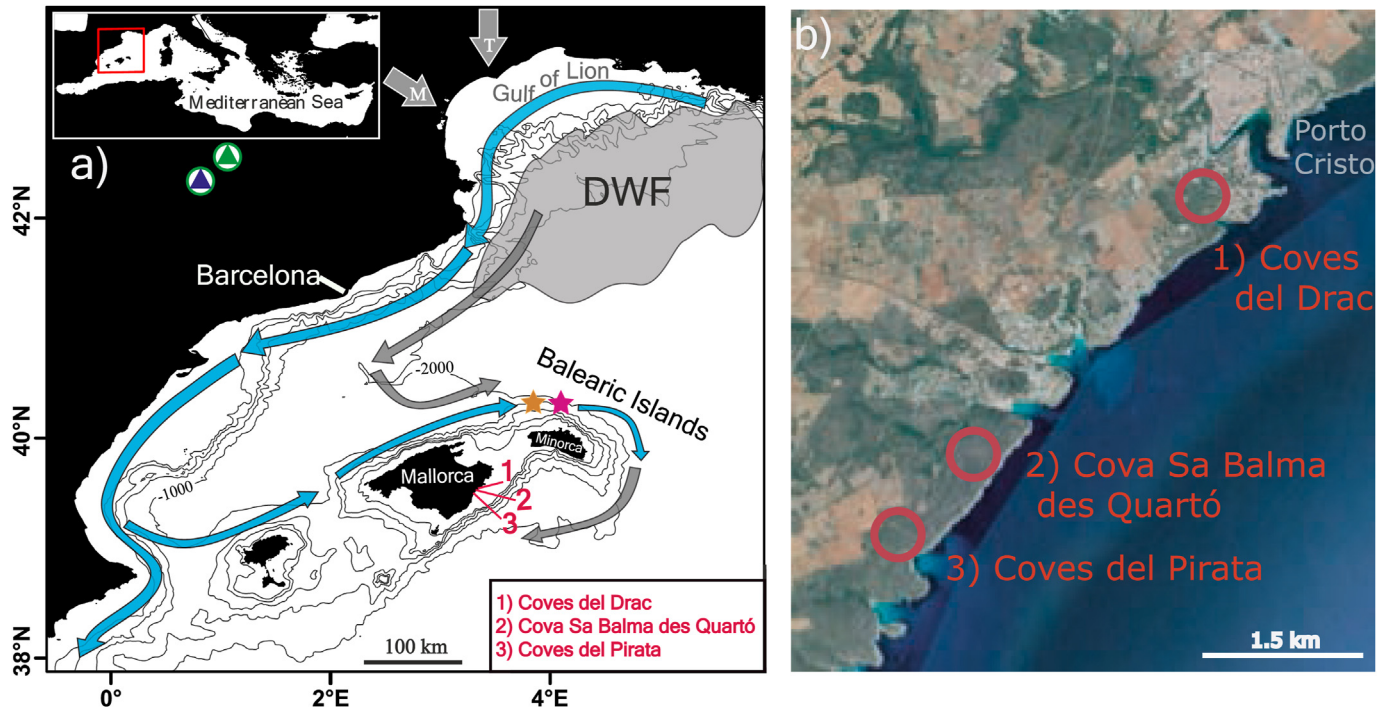


**Fig. 1.** Studied area **a)** Map of the central-western Mediterranean Sea with cave locations. Arrows over the Mediterranean indicate surface (blue) and deep (grey) circulation. Arrows over the Gulf of Lion indicate direction of the N-NW winds Tramuntana (T) and Mistral (M). Shallow area by the Gulf of Lion indicates where deep-water formation (DWF) occurs almost each winter. Also are indicated sites of other reconstructions from previous studies: orange and pink stars indicate MIN and MR3 marine sediment cores (Cisneros et al., 2016, 2019); green triangle corresponds to Basa de la Mora lake (Pérez-Sanz et al., 2013), blue triangle indicate Estanya lake (Morellón et al., 2009, 2011, 2011). **b)** Zoom of Mallorca east-coast with cave locations (this study). (For interpretation of the references to colour in this figure legend, the reader is referred to the Web version of this article.)

counted but the overall low drip rate of the cave often prevented their measurement. All the selected drip water sites originated in active soda-straw stalactites, which are abundant and particularly large in this cave. Recently precipitated calcite (farmed calcite) was recovered from glass plates located under the selected drip sites. Glass plates were located for approximately three months to represent main seasonal conditions, precise information on the placement dates for each glass slide is provided in Table S1a. Glass slides were located over growing stalagmites with a slight tilting, and geochemical measurements were performed on a homogenised sample of the whole calcite precipitate over the glass slide (7 × 5 cm). $CO_2$ and temperature measurements were measured during visits at two locations, the lower and upper part of the cave (Fig. 2b). Due to some technical complications, these measurements could not be taken routinely in each of the visits and this information is complemented with parallel measurements taken in the Drac Cave, at the Llac Delícies location (Fig. 3; Supplementary Table 1; Enseñat et al., 2019).

Dripping water was collected from the fastest dripping location in the cave (A0 station, Fig. 2a and b) during each visit. A parallel sampling of rain waters was performed during part of the cave sampling period (2015–2017) in the near location of Manacor (Moreno et al., 2021), analytical procedure was the same than that applied for the dripping water.

### 3.2. Sample description and XRD

This study is based on five stalagmites: Feni, Ciara, Multieix and Seán (from *Quartó* cave) and Constantine (from *Pirata* cave). Feni (15.5-cm-length), Multieix (30.5-cm-length), Constantine (9-cm-length) and Seán (12-cm-length) were found broken in their respective caves. The particular morphology and length of Multieix is similar to those remaining active stalagmites in a specific site of the cave, just where it was found, which suggests that it was recovered close of its growth position although its base was not identified (Fig. 2a). Ciara (42.5-cm-length) grew in the main chamber of *Quartó* cave and was found in-situ.

The stalagmites were cut into two halves and fabrics and discontinuities along the axial length were determined by optical microscopy of thin sections and acetate peels. Four thin sections were prepared for Multieix (3.4–6, 6–11.5, 15–20 and 20.5–23.5 cm) and one for Seán (4–6.5 cm). Acetate peels (Feldmann et al., 1989) were performed on Multieix stalagmite (0–3.4 and 23.5–30.5 cm) and also along all the other speleothems.

X-ray diffraction (XRD) measurements were performed on Multieix (3.5, 6.5, 11.5, 19, 23 and 28.5 cm) and Constantine (3.5, 6, and 7.5 cm) where changes in the mineralogy were observed using a Bruker D8-A25 diffractometer at the Geosciencies Barcelona (Institut GEO3BCN-CSIC). The diffractometer was equipped with a Cu tube (l = 1.5405 Å) and an ultrafast position sensitive detector (PSD). XRD scans were collected over the 2θ range between 3.5° and 65° with steps of 0.05° and an equivalent integration time of 576 s per step. A voltage (current) of 30 kV (40 mA) was applied to the X-ray generator. The phases in the samples were identified with Bruker's software package Diffrac.Suite™ together with the PDF-2 database from the International Centre for Diffraction Data (ICDD).

### 3.3. Age models

Stalagmite age models are based on a total of 62 U-Th ages performed according to the U and Th chemical procedures similar to those described in Edwards et al. (1987). Ages in Constantine stalagmite for 1.3–6.6 cm were performed in Xi'an Jiaotong University (China). The rest of ages were chemically prepared and

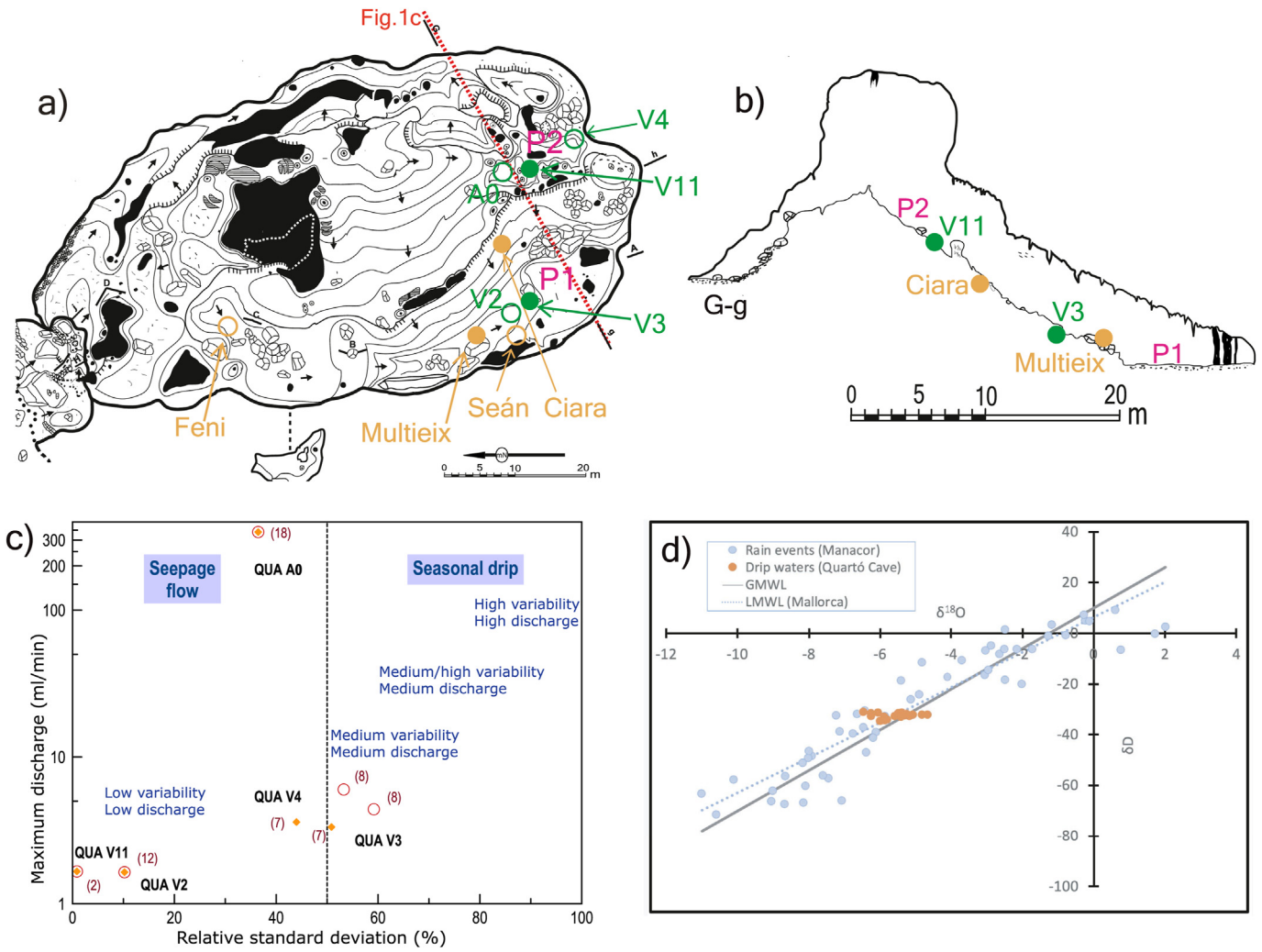


**Fig. 2.** Information about *Sa Balma des Quartó* cave. **a)** Topography from *Quartó* cave (Bermejo et al., 2014) with the location of the studied speleothems from this cave (filled circles indicate growth location; open circles indicate recovery location but not necessarily growth location), the location of the farmed calcite collected on glass plates (green filled circles, V3 and V11), and drip points A0, V2 and V4 (open green circles). P1 and P2 correspond to the lower and upper stations (respectively) were $CO_2$ concentrations were measured. Position of the vertical profile from Fig. 2b is also indicated. **b)** Vertical profile ('G-g' section in Bermejo et al., 2014) with the location of the speleothems recovered *in-situ*, the farmed calcite stations and the $CO_2$ measurement stations. **c)** Representation of the internal variability of the estimated dripping stations in *Sa Balma des Quartó* cave, in relation to its maximum discharge estimate (logarithmic scale) indicating the boundary that is considered to separate seepage flow from seasonal drip. The number of individual measurements is given in brackets. Stations V3 and V4 with an open circle represent the results considering the total number of measurements and with a filled circle those after the removal of one measurement (20/10/17) that introduced a large % of deviation. **d)** Dripping $\delta^{18}O$ data plotted in relation to the global meteoric water line and also the local one based on rain measurements recently published (Moreno et al., 2021). (For interpretation of the references to colour in this figure legend, the reader is referred to the Web version of this article.)

measured at University of Minnesota (USA). Analyses were conducted with a multicollector ICP-MS (Neptune Thermo Finnigan) following previously described methods (Cheng et al., 2013). To calculate the corrected ages in conjunction with the decay constant (Cheng et al., 2013) an initial $^{230}Th/^{232}Th$ atomic ratio of $(4.4 \pm 2.2) \times 10^{-6}$ was used (Table S.2). Individual age-depth models have been produced using the R statistics package Bchron (Parnell et al., 2008). Age model of the $\delta^{18}O$ composite record has been elaborated in the ISCAM software (Fohlmeister, 2012) in which individual age-depth models have been also obtained (see Section 3.5).

### 3.4. Trace element and stable isotopes analysis

Samples for trace element, $\delta^{18}O$ and $\delta^{13}C$ analyses were manually microdrilled at 1 mm intervals along the growth axis using a 0.5 mm diameter tungsten carbide dental bur. From the same carbonate sub-sample drilled in each discrete hole, around 1 mg was used to trace element analysis and around 60 μg to stable isotopes.

Trace elements were measured on an inductively coupled plasma mass spectrometer (ICP-MS, PerkinElmer ELAN 6000) in the Scientific and Technological Centres of the University of Barcelona (CCiT-UB). Samples were dissolved in 5 ml of dilute nitric acid (1 %; Tracepur) with Rh as an internal standard immediately before analyses. A standard solution was used for sample standard bracketing as a correction for instrumental drift, which was prepared gravimetrically with known concentrations of Ca, Mg, Sr and Ba, and it was produced with a ratio (element/Ca) comparable to that expected for the samples. The mean external reproducibility (2σ) for Sr/Ca, Mg/Ca and Ba/Ca ratios was 3.85 %, 4.00 % and 12.30 %, respectively, which are in agreement with previous publications (Torner et al., 2019), and for Al/Ca in Constantine stalagmite was 23.4%. To calibrate the obtained intensity ratios, six solutions with a

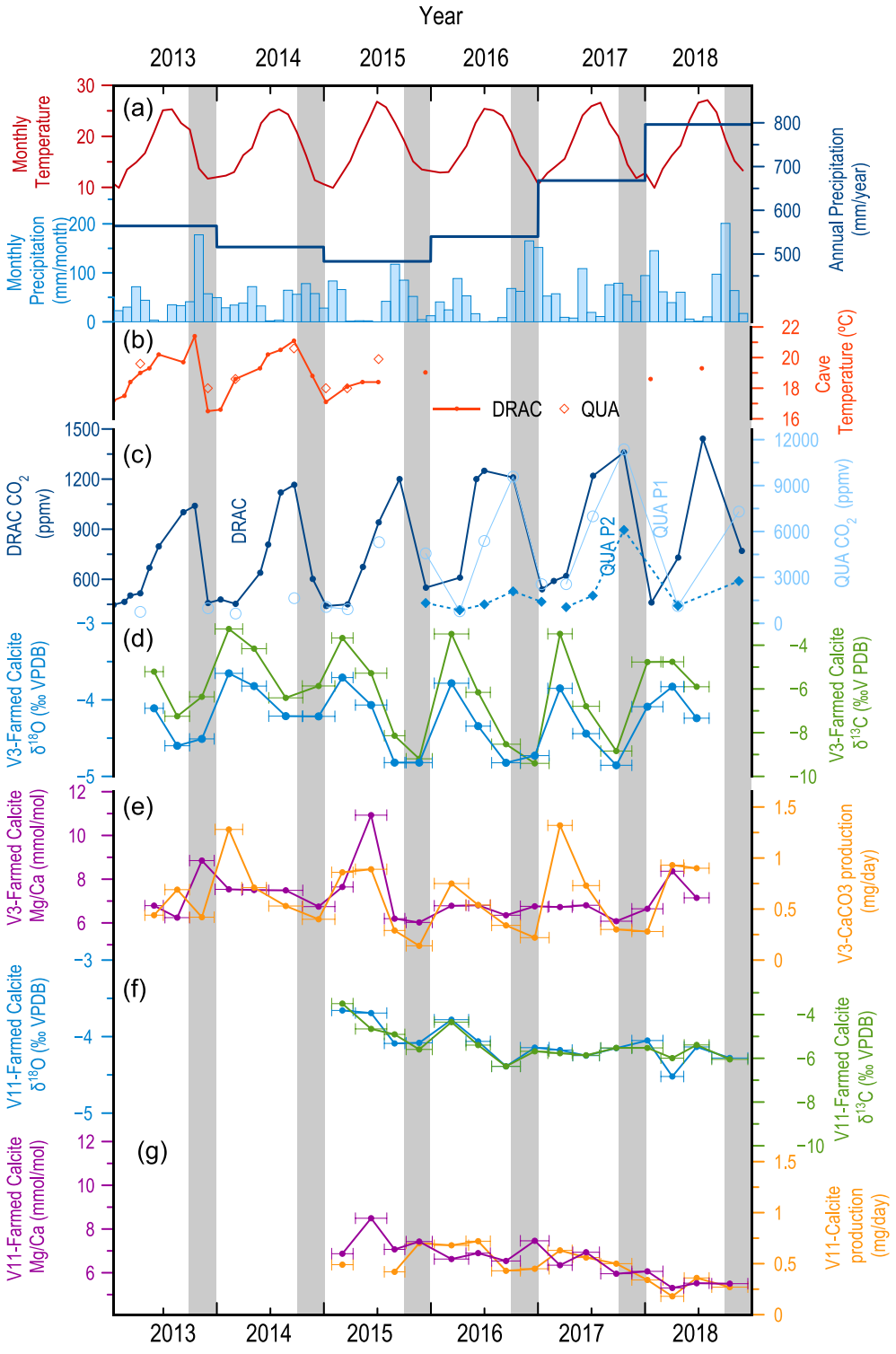


**Fig. 3.** Results from the monitoring exercise performed in *Sa Balma des Quartó* cave from April 2014 to November 2018. **a)** Monthly averages of air temperature (red) and monthly (light blue) and annual (dark blue) accumulated precipitations from a meteorological station close to the studied cave (Porto Colom, Balears Meteo: http://www.balearsmeteo.com/portocolom/wxindex.php). **b)** Punctual temperature measurements taken inside the caves, data from Quartó and Drac caves. **c)** Punctual $CO_2$ measurements taken inside Drac cave (dark blue) and in two different locations from Quartó cave, the lowest part of the cave (P1 – light blue) and the upper part of the cave (P2 – blue dot line), locations of P1 and P2 indicated in Fig. 2. Vertical axis is different for each cave. **d)** Stable isotopes ($\delta^{13}C$ and $\delta^{18}O$) measured in farmed calcite from station V3 (lower part of the cave). **e)** Mg/Ca ratios and calcification rates measured in farmed calcite from station V3 (lower part of the cave). **f)** Stable isotopes ($\delta^{13}C$ and $\delta^{18}O$) measured in farmed calcite from station V11 (upper part of the cave). **g)** Mg/Ca ratios and calcification rates measured in farmed calcite from station V11 (upper part of the cave). Horizontal lines in e-g located over each measurement indicate the time period of carbonate precipitation represented by each sample. Vertical grey bars indicate the autumn season for each studied year as reference. (For interpretation of the references to colour in this figure legend, the reader is referred to the Web version of this article.)

different trace element ratios values and a constant Ca concentration of 100 ppm were used. Stable isotope values were measured using a Finnigan MAT 252 mass spectrometer fitted with a Kiel-II carbonate microsampler in the CCiT-UB. The reproducibility was of 0.02‰ for $\delta^{13}C$ and 0.06‰ for $\delta^{18}O$. Calibration to Vienna Pee Dee Belemnite (VPDB) was carried out by means of NBS-19 standards.

Stable isotopes in dripping waters were also analysed at the CCiT-UB, δD via a thermal conversion elemental analyzer (TCEA) for pyrolysis coupled to a Thermo Delta Plus XP mass spectrometer, and $\delta^{18}O$ with a MAT 253 Thermo Fisher spectrometer coupled with a gas bench. Results are expressed per mill (‰) relative to Vienna Standard Mean Ocean Water (VSMOW). The analytical error for $\delta^{18}O$ and δD was ±0.2 ‰ and ±1.5‰, respectively.

### 3.5. PCA and $\delta^{18}O$ composite record

PCA and bivariate correlation (Pearson's) were performed with the statistical software Statgraphics for each set of records ($\delta^{18}O$, $\delta^{13}C$, Mg/Ca, Sr/Ca and Ba/Ca) with the age-depth model performed in Bchron to assess the common variability and explore the controlling environmental processes. Previously, trace element and stable isotopes records of each stalagmite in its own time-step were smoothed using a simple moving average of 5 terms and also normalized using standard methods (for each proxy and stalagmite). PCA median of all stalagmites was constructed after re-scaling each stalagmite record to a common time-step (8 years).

The $\delta^{18}O$ composite record has been constructed for the five stalagmites in the ISCAM software (Fohlmeister, 2012) applying a smoothing of 25 years, which takes into account ages and uncertainties of each stalagmite. The ISCAM method is implemented in MATLAB and uses a Monte Carlo approach on absolute age determinations to find the best correlation between climate proxies of several signal reproducing adjacent archives. Stalagmite individual records have been detrended, and normalized. Due to the absence of data in all stalagmites during part of the MCA-LIA, the composite record has been performed in two sections. The section spanning the oldest part includes Feni, Ciara, Multieix and Constantine records, while the most recent part includes Multieix and Seán records. In order to improve the correlation between records according to ISCAM simulations, seven ages of Ciara stalagmite and the oldest age of Constantine have not been included in the construction of the composite record (Table S2). Individual age-depth models performed on ISCAM, elaborated during the composite record construction are plotted together with those performed on Bchron in Fig. S5.

## 4. Results

### 4.1. Monitoring exercise

This monitoring exercise took place from 2013 to 2018 in *Quartó* Cave. Minimum averaged precipitations occurred during 2014 and particularly during 2015, while 2017 and 2018 were relatively wet years (Fig. 3a and b). Temperature and $CO_2$ measurements taken in *Quartó* and Drac cave show a strong seasonal cycle, with temperature oscillations of about 5 °C and parallel $CO_2$ changes in both caves (Fig. 3a). The amplitude of the $CO_2$ cycle is far lower (400–1400 ppm) in Drac cave than that of *Quartó* cave, which reaches maximum values on the lowest part of the cave (640–11370 ppm) while they were significantly reduced in the upper part (860–6100 ppm), although still high compared to the Drac cave values. *Quartó* cave has a very narrow access located at the upper part of the cave that should limit its ventilation while Drac cave has a far larger and more open access. Results indicate that annual cave ventilation starts to become more effective by the end of the autumn season, being winter and spring the two most ventilated seasons (Fig. 3c).

*Quartó* cave is a rather dry cave with very limited active dripping points; five of them were counted on a seasonal basis during the five studied years, although extreme low drip rates occasionally prevented its measurement (Table S1). Results indicate an overall low discharge and variability character, typically of dominant seepage flow (Fig. 2c). Overall, the drip rates show a subdued response to seasonal changes in hydrological conditions but they present some response to the major observed changes. This is particularly clear in the fastest drip point of the cave (A0; Table S1), where minimum values are coincident with the driest period during the year 2015 and early 2016. The other monitored points recorded lower drip rates, some of them too low to be counted during part of 2015 and 2016 years, while an increase occurred in almost all the dripping points within 2017, when annual rain was significantly higher. $\delta^{18}O$ and δD were measured in dripping water samples collected at A0 station (Fig. 2) approximately every three months (Table S1a). These results show that the isotopic values of the cave dripping water do not fit within the global meteoric water line (GMWL) and nor even within the local meteoric water line (LMWL) estimated with rain samples (Fig. 3h) from the near location of Manacor (Moreno et al., 2021). The sample collection of rainwater was part of the here presented monitor exercise and they overlap in time with the cave sampling and also share the analytical procedure. The average $\delta^{18}O$ value of the dripping water is −5.6 ‰ VSMOW, ranging from −4.7 to −6.5 ‰ VSMOW (Table S1a).

Geochemical measurements were performed in farmed calcite from two locations, V3 and V11, corresponding to the lower and the upper part of the cave respectively (Fig. 2c; Table S1). V3 shows a strong seasonal signal in both oxygen and carbon isotopes with lighter values during the summer and autumn season (minimum values of - 4.8 and −9.46 ‰ VPDB for $\delta^{18}O$ and $\delta^{13}C$, respectively) and heavier values during winter and spring (maximum values of - 3.65 and −3.25 ‰ VPDB for $\delta^{18}O$ and $\delta^{13}C$ respectively), following very much the already described cave ventilation cycle (Fig. 3; Table S2c). Besides this seasonal variability, an interannual variability can also be observed with overall heavier values during the 2014 and 2015 years and slightly lighter values during 2016–2018 (Table S2d). The described seasonal cycle can also be observed in the Mg/Ca record and in the precipitation rates, indicating that most of the carbonate (about the 74 % of the annual production) precipitated during winter and spring months coincident with highest values in all the studied geochemical parameters. On another hand, V11 shows a more smoothed seasonal signal in both $\delta^{18}O$ and $\delta^{13}C$ records, which almost disappeared during the most humid interval (2017–2018). But, in this case, the interannual variability is better represented with the heaviest values during 2015 and early 2016 (maximum values of - 3.66 and −3.50 ‰ VPDB for $\delta^{18}O$ and $\delta^{13}C$ respectively) and the lightest ones mostly during 2017 and 2018 (minimum values of - 4.5 and −6‰ VPDB for $\delta^{18}O$ and $\delta^{13}C$ respectively) (this location was not monitored during 2013 and 2014). This interannual difference is thus almost an order of magnitude larger in the geochemical parameters measured in V11 (upper part of the cave) than in V3 (lower part of the cave) although when the annual averaged values are weighted for the relative seasonal carbonate production, the amplitude of the interannual variability between the two sites is more comparable, particularly for $\delta^{18}O$ and Mg/Ca (Table S1; Fig. 3).

### 4.2. Fabrics and morphological features

On the basis of morphological structures and fabrics for each of the stalagmites, we have defined unconformity bounded units (UBUs), following Martín-Chivelet et al. (2017). Feni and Ciara

stalagmites have only one UBU, while Multieix, Constantine and Séan can be described by three, four and two UBUs, respectively (Fig. 4; Fig. S1-S2; details in the Supplementary Material).

### 4.3. Age models

Bchron software (Parnell et al., 2008), which is based on a continuous Markov monotone stochastic process, is robust regarding age uncertainties but cannot accommodate known hiatuses (Roesch and Rehfeld, 2019). The evaluation of fabric, morphological structures and U-Th ages of all stalagmites (Fig. 4; Supplementary Figures S.1-S.2 & Table S.2) indicates a hiatus at 5 cm of Multieix (UBU1-UBU2 boundary). This situation required of the independent construction of an age model for each section.

All models provided by Bchron have the same statistical significance (95 % confidence interval). Two different strategies have been followed to select the final age models of each stalagmite. The first one, applied in those stalagmites dated at higher resolution (Ciara, Constantine and Seán) for its corresponding period of growing, consists in averaging all models provided by Bchron. Seán age model was performed in two parts to minimize uncertainties, from the top to the unconformity at 6 cm and from there to the bottom. One of the nine U-Th ages of this stalagmite (10 cm) was excluded since it enhanced the outlier probability of the adjacent dates. The second strategy, applied in Feni and Multieix, has been to select the age model that better fit to the stable isotope and trace element records of the coeval stalagmite with more robust age model. The selection of one or other strategy has had different implications regarding growth rates, which show smoother step changes in the case of the first strategy (Figures S.1-S.2). An example of the multy-proxy methodology followed is shown in Fig. 4 (Multieix and Constantine stalagmites).

The studied speleothem records span the last 2.7 kyr (Table 1) and include the following climate/historical periods (years expressed as BCE, before common era, and CE, common era): the Talaiotic Period (TP; until 123 yr BCE), the Roman Period (RP; 123 yr BCE-470 yr CE), the Early Middle Ages (EMA; 470–900 yr CE), the Medieval Climate Anomaly (MCA; 900–1275 yr CE), the Little Ice Age (LIA; 1275–1850 yr CE), and the Industrial Era (IE) as the most recent (more details in Cisneros et al., 2016).

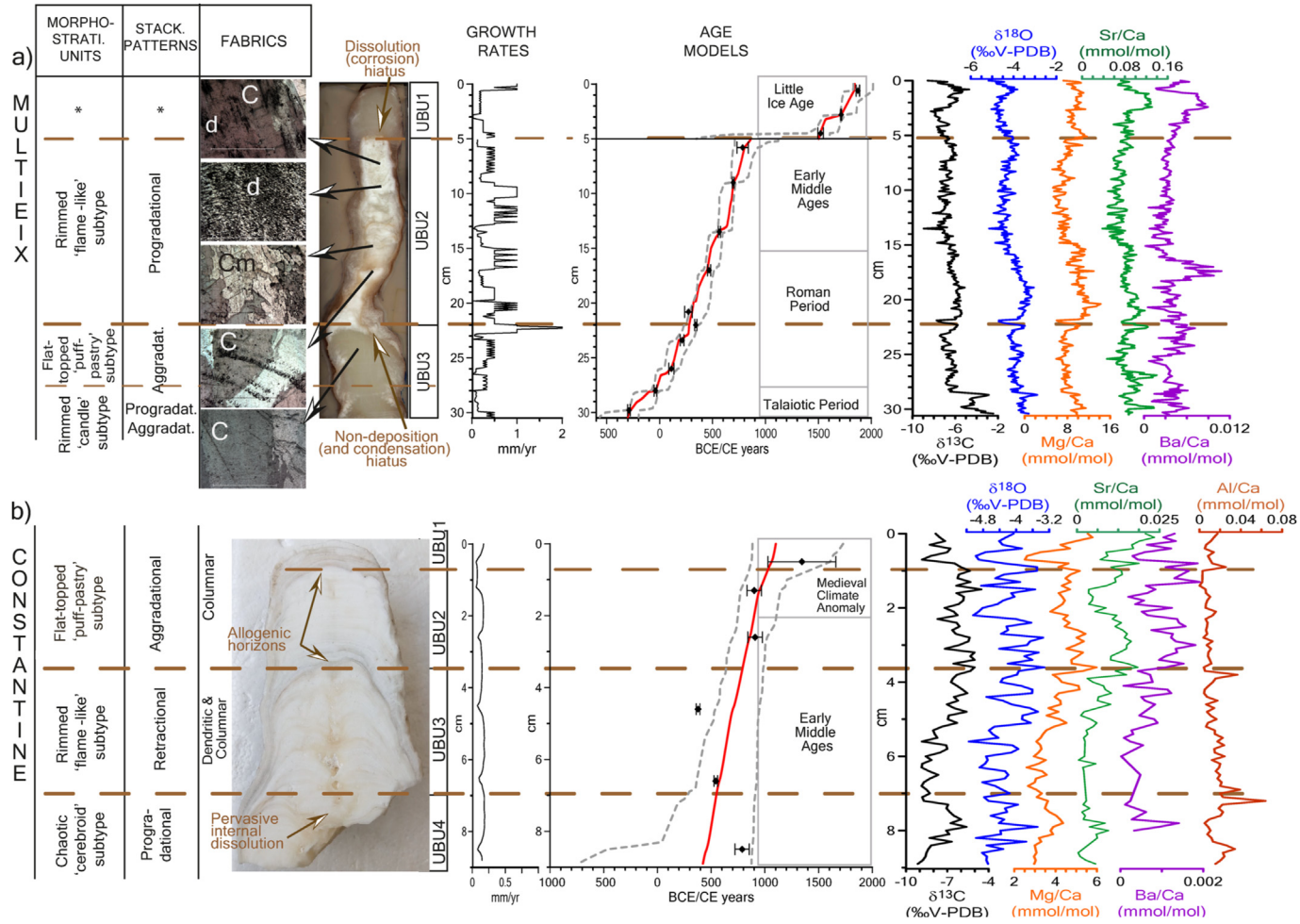


**Fig. 4.** From left to right: Schematic description of morphological features elements, stalagmite pictures, growth rates, U-Th age models, and stable isotope and trace element ratios records against cm for **a)** Multieix and **b)** Constantine stalagmites. U-Th age models performed on Bchron. Red plots are the final age models. Black diamonds represent the U-Th ages (error 2 sigma). Grey dashed lines correspond to uncertainties derived from all the age models obtained with Bchron, which have statistically the same significance. Ages are expressed in Before Common Era years (BCE) and Common Era years (CE). Historical/climatic periods are also indicated. Regarding to the fabrics of Multieix stalagmite (from bottom to top): Columnar fabric ('C', 23.5 cm), PPL; Open columnar fabric ('C', 17 cm), XPL; Columnar microcrystalline ('Cm', 15 cm), XPL; Dendritic fabrics ('d', 9.5 cm), PPL; Columnar fabric with dendritic branches (7 cm), XPL; Scale bar: 2 mm. (XPL = Cross Polarized Light; PPL = Plane Polarized Light). *Description of morphological features and details about U-Th ages of the top 5 cm in Multieix can be found in Fig. S2. (For interpretation of the references to colour in this figure legend, the reader is referred to the Web version of this article.)

**Table 1**
Stalagmites information on mean growth rates, mean time resolutions, and growth duration and source cave. More detailed information in Supplementary Material. *Considering the sampling resolution (1 mm). **Ranged from 37 to 1 years.

| Stalagmite | Mean growth rate (mm $yr^{-1}$) | Mean time resolution (yr)* | Duration of growth | Cave of growth |
|---|---|---|---|---|
| Feni | 0.8 | 2 | 653-301 yr BCE | Sa Balma des Quartó |
| Ciara | 0.7 | 2.2 | 537 yr BCE-398 yr CE | |
| Multieix (cm 30.5–5) | 0.4 | 4.6 | 302 yr BCE-858 yr CE | |
| Constantine | 0.1 | 7.6 | 423–1102 yr CE | Coves del Pirata |
| Seán | 0.4 | 3.8 | 1421–1880 yr CE | Sa Balma des Quartó |
| Multieix (cm 5-0) | 0.3 | 6.8** | 1503–1844 yr CE | |

### 4.4. Trace element records

Mg/Ca, Sr/Ca and Ba/Ca ratios have been determined for each stalagmite (Fig. 5; Table S3); Al/Ca was also measured in Constantine (Fig. 4). The highest mean Mg/Ca has been obtained in Multieix stalagmite (8.7 mmol $mol^{-1}$), while the highest mean Sr/Ca and Ba/Ca ratios are observed for Ciara (0.12 and 0.005 mmol $mol^{-1}$, respectively; Table S3). The lowest mean values of Mg/Ca, Sr/Ca and Ba/Ca (2.8, 0.1 $\times$ $10^{-3}$ and 4.1 $\times$ $10^{-3}$ mmol $mol^{-1}$, respectively) occur in Constantine stalagmite, which was found in a different cave than the rest of stalagmites. The ranges of the trace element ratios of stalagmites from *Quartó* cave are similar for each period. The range of the three trace element ratios of Constantine are different regarding the rest of stalagmites and Mg/Ca has the more similar range (Table S3).

The maximum values of Mg/Ca and Sr/Ca ratios have been obtained in Ciara (17 and 0.23 mmol $mol^{-1}$, respectively) at the end of the RP (Fig. 5), at which time are observed the highest Ba/Ca ratios in Ciara and Multieix (2 $\times$ $10^{-5}$ mmol $mol^{-1}$). The lowest ratios occur in Constantine for the beginning of the EMA and low values have also been obtained in Feni and Ciara stalagmites for the TP. Seán stalagmite also shows low Sr/Ca and Ba/Ca ratios during some moments of the LIA (Fig. 5).

Regarding to Al/Ca ratios measured in Constantine stalagmite, the average has been 1.4 $\times$ $10^{-2}$ mmol $mol^{-1}$. The maximum values have been obtained at ~460, 540, 770, and 1004 yr CE (ranging from 2.5 to 6.4 $\times$ $10^{-2}$ mmol $mol^{-1}$). Three of the peaks are coincident with the limit between the defined UBUs, which are characterized by allogenic horizons (at ~ 770 and 1004 yr CE) or by pervasive internal dissolution (at ~ 540 yr CE). The fourth peak corresponds to the oldest part of the stalagmite where pervasive internal dissolution has been also observed (Fig. 4; see Supplementary Material).

### 4.5. $\delta^{18}O$ and $\delta^{13}C$ records

The highest mean $\delta^{18}O$ and $\delta^{13}C$ values have been obtained in Multieix stalagmite (−4 and −6.4 ‰, respectively). The lowest mean of both isotopes corresponds to Seán (−5 and −8.5‰). The overall $\delta^{18}O$ variation ranges from 1.9 ‰ (Seán) to 2.3 ‰ (Ciara and Multieix) and for $\delta^{13}C$ from 6.4 ‰ (Multieix) to 2.3 ‰ (Feni) (Table S3).

The highest $\delta^{18}O$ and $\delta^{13}C$ values (−2.9 and −2.5 ‰, respectively) have been obtained in Multieix at the end of the TP and the lowest values in Seán (−5.9 and −10 ‰) during the LIA. High $\delta^{18}O$ and $\delta^{13}C$ values (~−3.2 and −4.2 ‰) have also been obtained in Ciara at the end of the RP and in Constantine during the MCA. By contrast, low $\delta^{18}O$ and $\delta^{13}C$ values (~−5.5 and −9.3 ‰, respectively) have also been obtained in Feni and Ciara during TP and beginning of the RP (Fig. 5).

The range of variation of the isotope values is consistent during the overlapping periods in all stalagmites, except in the older part of Multieix. This stalagmite did not grow continuously but it is particularly relevant in this study because it overlaps with most of the other studied stalagmites. For its lower unit of growth (UBU3; 279 yr CE-302 yr BCE), isotope records present the highest values, which are higher than those obtained in the coeval stalagmite Ciara (Fig. 5).

### 4.6. Principal component analysis (PCA)

PCA can be used to explore common variability and patterns between different data sets and the PCs often provide an easier interpretation than the original data sets (e.g. Mischel et al., 2016; Nagra et al., 2017). One PC is required to explain the data set of Ciara and Constantine stalagmites (86 % and 74 %, respectively), while two PCs are required in the case of Feni, Multieix and Seán. In these latter stalagmites, PC1 explains between 46 and 71 % and PC2 between 26 and 37 % (Fig. 6). Therefore, discussion is mostly based on PC1 in the following.

Trace element ratios and stable isotopes records have medium positive PC1 loading numbers in all stalagmites except in Seán (Fig. 6; Table S4). In Ciara, Feni, Constantine and Multieix, all PC1 loading numbers for trace element ratios and stable isotopes records have similar range from 0.3 to 0.5. In contrast, in Seán stalagmite Sr/Ca and Ba/Ca have low negative loadings (from −0.1 to −0.3) and $\delta^{18}O$ and $\delta^{13}C$ have higher positive loadings (0.6).

## 5. Discussion

### 5.1. Interpreting the geochemical signature in farmed calcite

One of the most outstanding results of recently precipitated calcite is the high correlation between the $\delta^{18}O$ and $\delta^{13}C$ measurements ($r \geq 0.9$, p *value* < 0.05) and to a lesser extent with the Mg/Ca ratio (Table 2). Cave precipitates and model data have demonstrated that under low rate drippings (typically of seepage drips), as is the case of Quartó cave (Fig. 2), oxygen and carbon isotopes tend to be incorporated in disequilibrium into the carbonate, resulting in heavier $\delta^{18}O$ and $\delta^{13}C$ values than those predicted for equilibrium (Riechelman et al., 2013). Measurements of $\delta^{18}O$ in dripping waters of Quartó cave provide average values of −5.6‰ VSMOW. The collected drip waters in Quartó cave are in disequilibrium with both the GMWL but also the LMWL (Fig. 3h) suggesting the existence of severe degassing and evaporation processes within the karst system that produce intense isotopic fractionation. In addition, the drip water $\delta^{18}O$ values (−5.33‰ when transferred into VPDB) show lighter values than those of the averaged farmed calcite (−4.2‰ VPDB). But, taking in account the relatively warm cave temperature (roughly 18.8 °C), carbonate $\delta^{18}O$ values should be about −6.3 ± 0.1‰ VPDB, if precipitation would occur in equilibrium with the dripping fluid (Craig, 1965; Anderson and Arthur, 1983). Consequently, cave evaporation, degassing and/or PCP processes should exert a strong effect in the calcite $\delta^{18}O$ signal.

The good co-variance between temperature and $CO_2$ values in both *Quartó* and also *Drac* caves (Fig. 3c) supports the control of

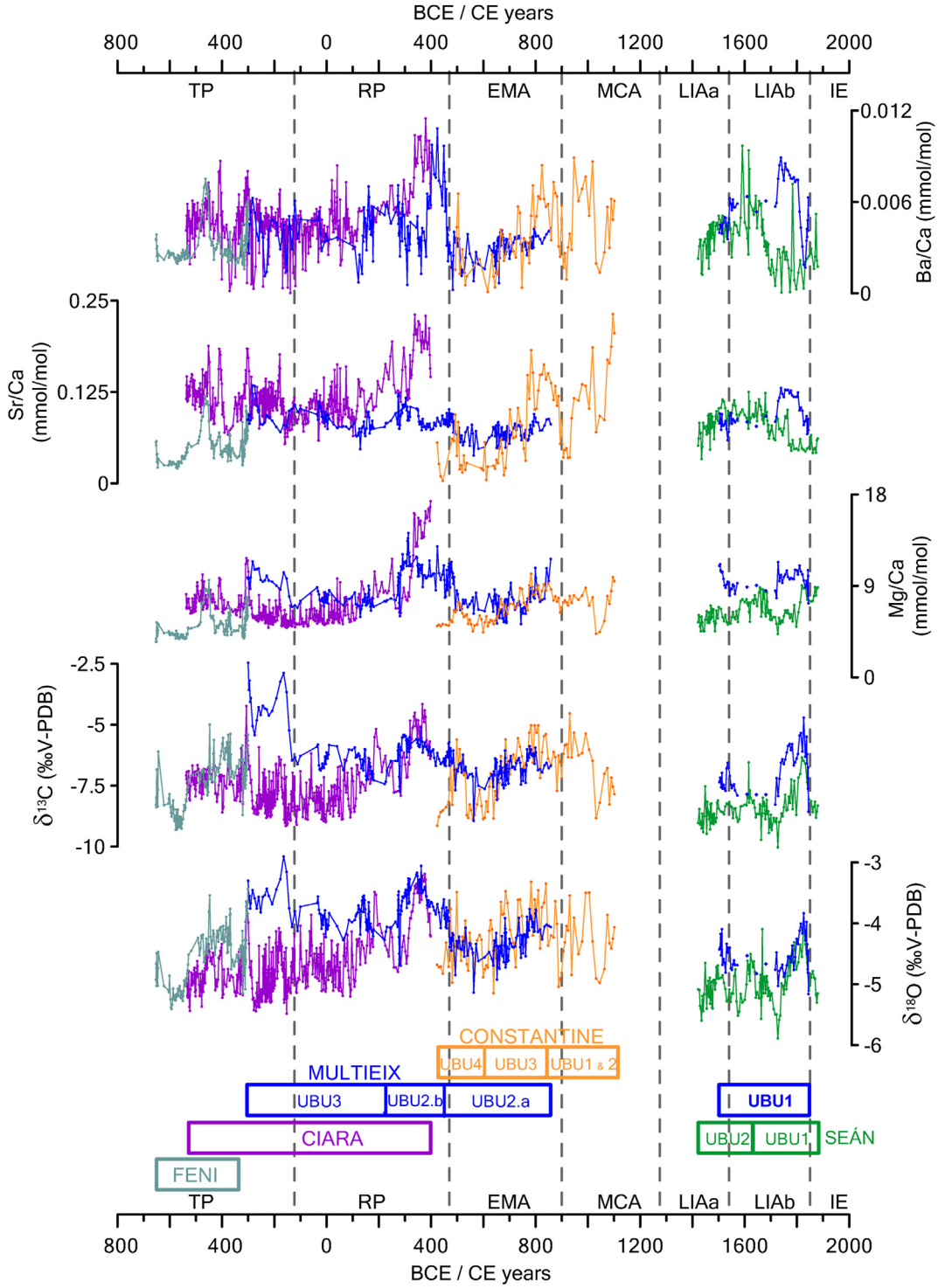


**Fig. 5.** From top to bottom: Ba/Ca, Sr/Ca, Mg/Ca, $\delta^{13}C$ and $\delta^{18}O$ records for stalagmites: Feni (light blue); Ciara (purple); Multieix (blue); Constantine (orange) and Seán (green). Constantine trace element ratios are normalized to the average value of the other four stalagmites; this is the only stalagmite from *Pirata* cave. The defined unconformity Bounded Units (UBU) for each stalagmite are also indicated in the lower part using the same colour code than geochemical records. Ages expressed in years Before Common Era (BCE)/ Common Era (CE). Information on the used 50 U-Th ages are in Table S2. TP: Talaiotic Period; RP: Roman Period; EMA: Early Middle Ages; MCA: Medieval Climate Anomaly; LIA: Little Ice Age; IE: Industrial Era. (For interpretation of the references to colour in this figure legend, the reader is referred to the Web version of this article.)

ventilation processes on the cave $CO_2$ concentration. This seasonal cycle is coherent with that also observed in both $\delta^{18}O$ and $\delta^{13}C$ values from V3 station, with heavier values when ventilation is maximum and coincident with maximum rates in carbonate production (Fig. 3). Variable drip rates have been identified in previous studies as the main control of isotopic disequilibrium (Riechelman et al., 2013). Nevertheless, drip rates in Quartó cave present very little seasonal variability and in any case, lower drops in drip rates were detected mostly in early autumn, when isotopes show their lightest values (Table S1a), the opposite trend to that expected for

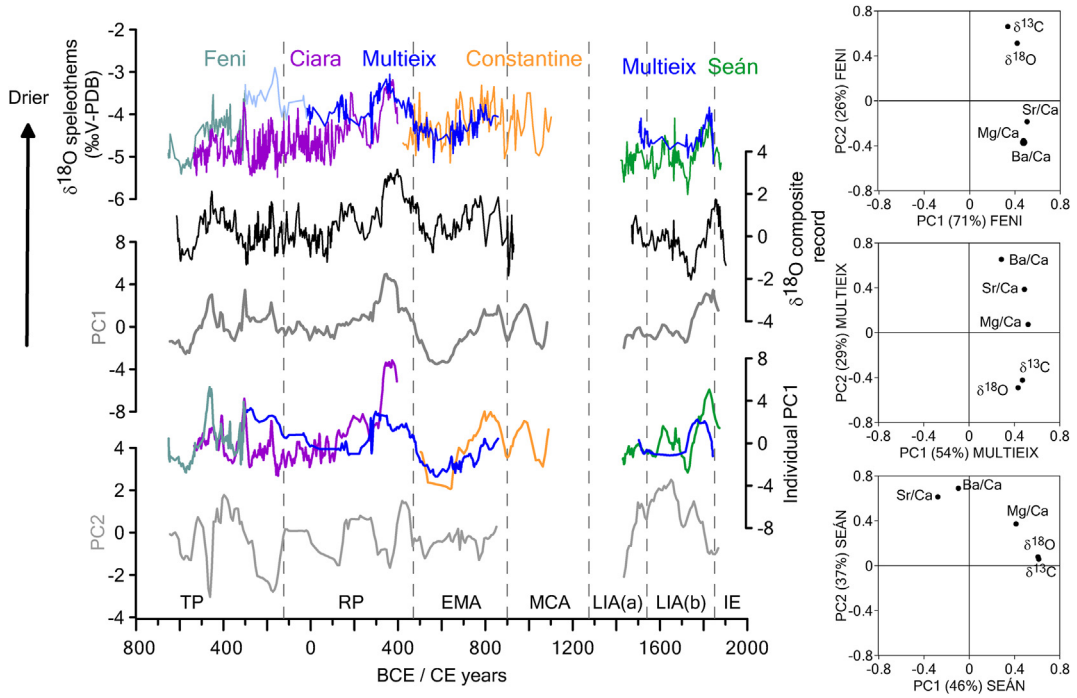


**Fig. 6.** Comparison of the $\delta^{18}O$ stalagmite records with the PCA results. Left panel (from top to bottom): $\delta^{18}O$ records from the five Mallorca stalagmites (light blue curve indicates the oldest part of Multieix not included in the composite record); $\delta^{18}O$ composite record (black); PC1 median conducted in each stalagmite records (dark grey); PC2 median (light grey). Right panel: loadings on PC1 and PC2 for Feni, Multieix and Seán stalagmites. In the case of Ciara and Constantine, PC1 explained the highest variance, 86 and 74 % respectively, while PC2 is not significant (eigenvalue <1; Full data in Table S4). (For interpretation of the references to colour in this figure legend, the reader is referred to the Web version of this article.)

**Table 2**
Coefficients of Pearson's correlation "r" between Mg/Ca with $\delta^{13}C$ and $\delta^{18}O$, respectively, for each stalagmite and separated by individual UBUs, and also for farmed calcite at V3 and V11 stations. (*) Correlations performed with records previously smoothed (simple moving average of 4 terms) to minimize the signal from the seasonal cycle, which is less marked in the Mg/Ca ratio than in the stable isotope records.

| Stalagmite, UBU or farmed calcite | $\delta^{18}O$ vs. $\delta^{13}C$ | | Mg/Ca vs. $\delta^{18}O$ | | Mg/Ca vs. $\delta^{13}C$ | |
|---|---|---|---|---|---|---|
| | R | *p* value | r | *p* value | r | *p* value |
| Feni | 0.90 | <0.05 | 0.61 | <0.05 | 0.51 | <0.05 |
| Ciara | 0.90 | <0.05 | 0.76 | <0.05 | 0.82 | <0.05 |
| Constantine | 0.68 | <0.05 | 0.57 | <0.05 | 0.75 | <0.05 |
| Multieix | 0.77 | <0.05 | 0.48 | <0.05 | 0.47 | <0.05 |
| Seán | 0.76 | <0.05 | 0.39 | <0.05 | 0.49 | <0.05 |
| All stalagmites | 0.80 | <0.05 | 0.53 | <0.05 | 0.57 | <0.05 |
| Constantine UBU1-2 | 0.62 | <0.05 | 0.58 | <0.05 | 0.46 | <0.05 |
| Constantine UBU3 | 0.83 | <0.05 | 0.66 | <0.05 | 0.86 | <0.05 |
| Constantine UBU4 | 0.72 | <0.05 | 0.42 | 0.08 | 0.81 | <0.05 |
| Mutieix UBU1 | 0.68 | <0.05 | 0.28 | <0.05 | 0.35 | <0.05 |
| Multieix UBU2 | 0.84 | <0.05 | 0.81 | <0.05 | 0.79 | <0.05 |
| Multieix UBU3 | 0.81 | <0.05 | 0.66 | <0.05 | 0.66 | <0.05 |
| Seán UBU1 | 0.81 | <0.05 | 0.38 | <0.05 | 0.54 | <0.05 |
| Seán UBU2 | 0.60 | <0.05 | 0.25 | 0.06 | 0.32 | <0.05 |
| V3 (farmed calcite) | 0.97 | <0.05 | 0.42 | 0.06 | 0.38 | 0.09 |
| V11 (farmed calcite) | 0.90 | <0.05 | 0.58 | <0.05 | 0.38 | 0.16 |
| V3 (farmed calcite)* | 0.99 | <0.05 | 0.77 | <0.05 | 0.76 | <0.05 |
| V11 (farmed calcite)* | 0.97 | <0.05 | 0.80 | <0.05 | 0.65 | <0.05 |

isotopic disequilibrium controlled by reduced dripping conditions. In this case, we propose that isotope disequilibrium associated to the seasonal cycles results from a Rayleigh distillation enrichment of both $^{18}O$ and $^{13}C$ in the $HCO_3^-$ of the dripping solution due to $CO_2$ degassing and calcite precipitation (Mickler et al., 2006; Riechelman et al., 2013). But the rate of $CO_2$ degassing should be controlled by the cave $CO_2$ concentration and not by dripping rates that maintained slow along the year (Carlson et al., 2020). V3 station is located in the lower part of the cave where the $CO_2$ cycle shows the largest amplitude according to in situ measurements, reaching maximum values (6000–11,300 $ppm_v$) during the poorly ventilated period (Fig. 3). We propose that isotopic disequilibrium that led to the seasonal cycle in V3, was controlled by the cave $CO_2$ concentrations in contrast to other cave studies where water drip degassing is mostly controlled by variable drip rates (Riechelman et al., 2013). These extremely high $CO_2$ concentrations during summer and autumn in the lowest part of the cave (V3 location) prevented degassing processes, reducing isotope fractionation

(lightest $\delta^{18}O$ and $\delta^{13}C$ values) and also reducing calcification rates (Carlson et al., 2020). On the contrary, during winter and spring months cave air $CO_2$ values decreased, enhancing the degassing processes and thus isotope fractionation (heavier isotopes) while carbonate precipitation rates also increased (Fig. 3). It should be noted that, if seasonal changes in degassing intensity would have been controlled by changeable dripping rates, an opposite relation should be expected within isotopic ratios and calcification rates (Riechelman et al., 2013; Carlson et al., 2020). The different location of V11 station, in the upper part of the cave, where the amplitude of the seasonal $CO_2$ cycle is significantly lower, would explain why the seasonal cycle is less intense in the carbonates precipitates recovered at this site location (Fig. 3).

Overprinting to the above described seasonal cycle, geochemical results on farmed carbonates also show an interannual variability at both V3 and V11 stations, although the amplitude appears to be larger in this last station, which is also the less affected by the seasonal degassing cycle. Both stable isotopes and Mg/Ca ratios present averaged higher values during the drier years (2014–15) than during the wetter ones (2017–2018) (Fig. 3; Table S1d). In the case of V3 station, carbonate precipitation rates present significant changes associated to the seasonal cycle (Fig. 3) and when annual averaged geochemical values are weighted for their seasonal carbonate contribution (Table S1b), the differences between the dry and wet years are more comparable between the two studied stations. According to the observed evolution in the drip rates of Quartó cave, an overall dripping rate reduction occurred during the drier period (Table S1.a). Lower drip rates would enhance PCP that will increase trace elements in the dripping solution but also enhance kinetic isotopic fractionation in the epikarst and cave by enhanced Rayleigh distillation that would led into heavier $\delta^{18}O$ and $\delta^{13}C$ values (Johnson et al., 2006; Fairchild and Treble, 2009). Unfortunately, the scarce data on the time evolution of dripping rates in V3 site are inconclusive to support this as the control factor. Alternatively, processes acting on the soil layer could also exert a comparable control on the analysed geochemical parameter. Increased soil activity would raise the $pCO_2$ of the infilling waters and ultimately on cave dripping waters, weakening the $pCO_2$ gradient with cave air and thus degassing processes (Kaufmann and Dreybrodt, 2004). Since soil activity in this Mediterranean climate is controlled by water availability, the effect of degassing intensity led by changeable $pCO_2$ on the isotopes and trace elements would also reflect regional hydrological changes (Mühlinghaus et al., 2009; Kaufmann and Dreybrodt, 2004). Consequently, we propose that even though the seasonal signature of the studied chemical parameters does not reflect annual changes in the Mallorca hydrology, interannual variability in average precipitation become recorded into the cave carbonate, by controlling drip rates intensity and thus associated PCP and/or soil activity control on $pCO_2$. This would explain the extremely high covariance between the two stable isotopes signals ($\delta^{13}C$ and $\delta^{18}O$) and Mg/Ca ratios for the interannual variability (Fig. 3 and Table S1). Therefore, this monitoring data support that speleothem records from *Quartó* cave archive a valuable hydrological signature at multiannual time scale (Table 2 and Table S3).

### 5.2. Control factors on trace element and stable isotope stalagmites records

According to the age models and the morphological features, most of the stalagmites grew continuously during the last 2.7 kyr without important signs of erosion except the hiatus in Multeix (growth stopped between 850 yr CE and 1503 yr CE; S3.3 in Supplementary Material). Morphostratigraphic units have been described as flat-topped type in some parts of all stalagmites, while rimmed type is also present in Feni, Multeix and Constantine stalagmites, which are in agreement with a general continuous calcite growing during the spanned period (Fig. 4; S1-S2). The main morphological features described in individual stalagmites show frequently common patterns during coeval periods (see Supplementary Material). For instance, Multeix and Constantine are characterized by rimmed 'flame-like' subtype during the EMA (Fig. 4). All the stalagmites show distinctive changes in the predominant stacking patterns (progradational, aggradational, retractional), which are commonly associated to decadal to centennial variations. It should be noted that due the vertical component always present in the growth of a stalagmite, all the stacking patterns have some aggradational component, so no "pure" progradational nor "pure" retractional patters can be expected (Martín-Chivelet et al., 2017). According to observations of the predominant stacking patterns in the stalagmites, trends to increasing drip rates (progradational patterns) seem to have been frequently accompanied by trends to more depleted $\delta^{18}O$ values as occurs in Ciara during the early RP or in Constantine during the beginning of the EMA (Fig. 5 and S1). These observations support the sensitivity of the studied speleothems to decadal to centennial climatic-hydrological changes in Mallorca.

The $\delta^{18}O$ and $\delta^{13}C$ records in the studied stalagmites show a high covariance with high Pearson's correlation coefficients ($r \geq 0.7$, $p$ *value* $< 0.05$; Table 2; Fig. S3) as it was the case for the farmed calcite (Fig. 3; Table 2). As it has already been discussed in section 5.1 this situation is often attributed to an isotopic disequilibrium during carbonate precipitation (Riechelman et al., 2013) questioning its value as paleoclimatic records. Accordingly to the discussed results from farmed calcite, we argue that speleothem $\delta^{18}O$ and $\delta^{13}C$ signals are intimately linked to the regional hydrology, by controlling drip rates intensity and thus associated PCP and/or soil activity control on $pCO_2$. The discussed seasonal variability in the farmed calcite should not be captured by the speleothem records since temporal resolution of the geochemical analyses ranges from 2 to 7 years (Table 1). The additional good covariance between the Mg/Ca, Sr/Ca and Ba/Ca ratios of the stalagmites (Pearson's correlation coefficients (r) from 0.32 to 0.94; Table 3) and of the Mg/Ca ratios with the isotopic records (r ranging from 0.47 to 0.82; Table 2), is in agreement with enhanced concentration in the drip solution of trace metals due to PCP (Treble et al., 2003; Fairchild and Treble, 2009; Moreno et al., 2010; Bartolomé et al., 2015; Pérez-Mejías et al., 2017, 2019). PCP is expected to increase under dry climate conditions because longer water residence time in the epikarst and decreased drip rates enhance contact of the water with a lower $pCO_2$ environment, leading to prolonged duration of $CO_2$ degassing and $CaCO_3$ precipitation before the drop arrives at the stalagmite top (Fairchild et al., 2000).

Following additional tests proposed by Sinclair et al. (2011) for the interpretation as PCP-driven in the trace element ratios, the logarithmic relationship between Mg/Ca and Sr/Ca ratios has been explored. The logarithmic relationship of all dataset except Seán (Supplementary Material) has shown a slope of 1.5, which is in

**Table 3**
Coefficients of Pearson's correlation "r" between the three trace element ratios for each stalagmite.

| Stalagmite | Mg/Ca vs. Sr/Ca | | Mg/Ca vs. Ba/Ca | | Sr/Ca vs. Ba/Ca | |
|---|---|---|---|---|---|---|
| | R | *p* value | r | *p* value | r | *p* value |
| Feni | 0.84 | <0.05 | 0.82 | <0.05 | 0.94 | <0.05 |
| Ciara | 0.78 | <0.05 | 0.67 | <0.05 | 0.72 | <0.05 |
| Constantine | 0.72 | <0.05 | 0.61 | <0.05 | 0.68 | <0.05 |
| Multeix | 0.59 | <0.05 | 0.32 | <0.05 | 0.55 | <0.05 |
| Seán | −0.03 | 0.78 | 0.15 | 0.11 | 0.66 | <0.05 |

agreement with those pointed out in Wassenburg et al. (2020) corresponding to PCP control (range values between 0.7 and 1.5). In Ciara and Multieix (without the oldest part of the record) has been obtained a slope of 0.7 and in Feni a slope of 1.5. The slope between ratios obtained in Constantine (2.5) is higher than those of the range corresponding to the PCP test but still near of those obtained in other stalagmites shown in Sinclair et al. (2010). Higher slopes can be attributed to detritus material input (Sinclair et al., 2012). It should be noted that the logarithmic test has been performed in all the dataset of Constantine that corresponds to a different cave and, in which have been detected allogenic horizons (Supplementary Material). Therefore, we conclude that geochemical records in the studied speleothems should reflect humidity and thus become a good proxy of annual averaged changes in the precipitation patterns of Mallorca. Nevertheless, the existence of a common hydrological control among the different studied geochemical records is further tested by statistically analyses.

Results from the PCA statistical analysis present a PC1 that can explain most of the variability for all five speleothems, particularly in Feni, Ciara and Constantine where the common variability explained by PC1 range from 86 to 71 % (Fig. 6 and Table S4) while in Multieix and Seán it explains up to the 54 and 46 % of common variability respectively. In contrast, the PC2 explains far lower percentage of variability, 37 to 26 % in Seán, Multieix and Feni, and is not significant in Constantine and Ciara (eigenvalue <1; Fig. 6 and Table S4). These results support that among the several complex factors that can account for the speleothem geochemical signal, it exists a dominant one that can be explained by the PC1. We suggest that factor to reflect the previously argued PCP control over the different geochemical proxies.

The individual loadings within the PC1 are very comparable for most of the analysed parameters with the exception of Seán where Sr/Ca and Ba/Ca ratios show negative numbers (Table S4), while Mg/Ca show closer loading values to the stable isotopes ($\delta^{18}O$ and $\delta^{13}C$). These observations suggest that some other processes had a major effect controlling Sr and Ba incorporation during Seán growth and that also would explain why Seán is the speleothem with a higher weight of the PC2. It is also interesting to remark that within the PC2 the load of Sr/Ca and Ba/Ca ratios in the whole set of speleothems is always very different than that from $\delta^{18}O$ and $\delta^{13}C$ while Mg/Ca values mostly locates between them. Growth rates can produce a strong kinetic control on both Sr and Ba that is not observed in Mg (Stoll et al., 2012). That effect could be relevant particularly in Seán, where relatively low Sr/Ca and Ba/Ca ratios at the upper part could be explained by the higher growth rates of this UBU1 (1622–1880 yr CE) (Fig. 6; S3.1; S4).

Consequently, stable isotopes appear to have a homogeneous load on the PC1 among the five studied speleothems, supporting the dominant control of a single factor that, according with the previous discussion, we interpret mostly to reflect PCP changes driven by variable drip rates associated to regional hydrology.

### 5.3. $\delta^{18}O$ Mallorca stalagmite composite record: 2.7 kyr hydroclimate variability

As discussed above, a series of evidences from our results point out that the $\delta^{18}O$ speleothem records are robust indicators of regional hydrological conditions, and that this proxy illustrates the variability of the main factor controlling the chemical signature of the speleothems, i.e. PCP. Further support comes from: the preferential $^{18}O$ incorporation shown by the farmed calcite during the driest monitored years (2014–2015); the good agreement between $\delta^{18}O$ and the described morphological features; the very comparable $\delta^{18}O$ values among the different speleothems (−3 to −6‰), including the one from a different cave, and between the different *Quartó* stations for farmed calcite (−3.5 to −4.9‰). As a consequence, we have chosen $\delta^{18}O$ records to produce a composite record, which includes the five studied speleothem records with the only exception of the oldest part of Multieix stalagmite (UBU3, 302-19 yr BCE), which is argued in the supplementary material (S3.2). The resulting $\delta^{18}O$ composite record, as expected, is in good agreement with the PC1 mean record of all stalagmites ($r = 0.56$; $p\ value < 0.05$; Fig. 6). According to our previous interpretations, $\delta^{18}O$ in these speleothems mostly reflects PCP changes associated to variable drip rates, controlled by precipitation changes. Consequently, higher (lower) $\delta^{18}O$ values are interpreted as drier (wetter) conditions in the region in terms of moisture balance. According to the farmed calcite results, interannual variability in recharge or precipitation becomes reflected into the chemistry of the cave carbonate due to PCP processes associated to variable drip rates or soil activity as discussed above.

The resulting composite record (Fig. 7) indicates rather wet conditions for most of the TP, the earlier part of the RP, most of the EMA and the LIA, particularly the LIAb appears as one of the wettest periods. In contrast, driest conditions are observed particularly during the last part of the RP, to less degree by the end of the EMA, and during the transition from the LIAb to the IE (Fig. 7 and S4). The MCA is represented by a hiatus in our composite record that could suggest the dominance of extreme dry conditions in the region in agreement with the observations from a previous compilation effort of paleoclimatic records from the Iberian Peninsula (Moreno et al., 2012). According to the farmed calcite collected on glass plates, driest years with an average annual precipitation of 500 ml presented carbonate $\delta^{18}O$ values of −4.2‰ while the wettest years with annual precipitation averages of 730 ml have values of −3.9 ‰ (Table S1c-d). Although a direct calibration with precipitation values cannot be established, this comparison provides a framework to evaluate the intensity of the precipitation changes during the last 2.7 kyr. Thus, the observed $\delta^{18}O$ evolution would suggest changes significantly larger than those covered during the monitored period, locating this between a rather dry period within the last 2.7 kyr. Nevertheless, a complete IE coverage by our record, or a larger monitoring window is missing to establish a more solid comparison between the paleorecord and the observation period. The $\delta^{18}O$ composite record is compared with other paleoclimatic and paleoceanographic records to obtain a regional overview of past hydrological conditions.

### 5.4. The last 2.7 kyr in the central-western Mediterranean region

The hydroclimate variability interpreted in base to the $\delta^{18}O$ composite record produced in this study is compared with previously published reconstructions derived from marine sediments from the same area and for the same period: (i) SST based on Mg/Ca analysed on the planktonic foraminifera *Globigerina bulloides* (Cisneros et al., 2016); and (ii) Deep Water Formation (DWF) variability in the Gulf of Lions based on the grain-size parameter UP10, which corresponds to the fraction coarser than 10 μm and can be used as a proxy of deep-current variability (Cisneros et al., 2019). This comparison shows that dry conditions in Mallorca, represented by heavier $\delta^{18}O$ values in the Mallorca composite record, occurred during both warm and cold periods indicated by SST variations (Fig. 7). This complex relationship is well illustrated when RP and EMA periods are compared. During RP climate conditions evolved from cold and wet to warm and dry while during the EMA, climate migrated from warmer/wetter conditions to colder/drier conditions (Fig. 7). These observations highlight the complexity in the climatic response of the region and also suggest the RP and EMA transition as a period of breakdown in the operation mode of the regional climate variability (Cisneros et al., 2019).

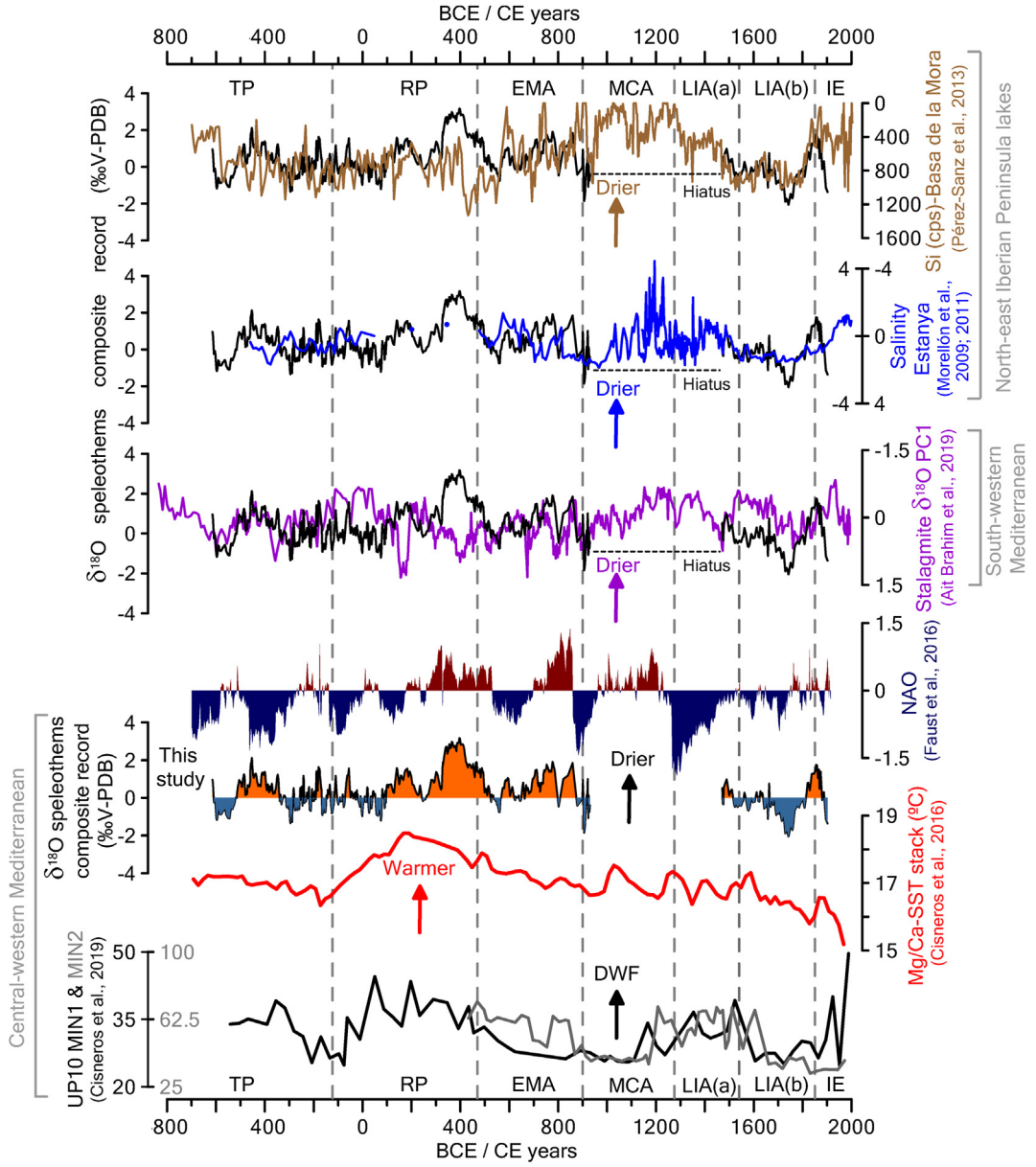


**Fig. 7.** From top to bottom: Mallorca $\delta^{18}O$ composite record (black and hiatus indicated with black dashed horizontal line) compared with run-off reconstruction (brown) from Basa de la Mora Lake (Pérez-Sanz et al., 2013); with a Salinity reconstruction (blue line) from Estanya Lake in the north-eastern Iberian Peninsula (Morellón et al., 2009, 2011); and PC1 conducted in $\delta^{18}O$ records (purple) from Morocco stalagmites (Ait Brahim et al., 2019). North Atlantic Oscillation (NAO) reconstruction (Faust et al., 2016); Mallorca $\delta^{18}O$ stalagmite composite record (this study); Sea surface temperature (SST) composite from central-western Mediterranean based on Mg/Ca ratios measured on *Globigerina bulloides* (Cisneros et al., 2016). The grain size parameter UP10 as a proxy of Deep-water formation (DWF) in the Gulf of Lion (core MIN1 in black, core MIN2 in dark grey from Cisneros et al., 2019). (For interpretation of the references to colour in this figure legend, the reader is referred to the Web version of this article.)

Regarding the relationship of the $\delta^{18}O$ composite with the proxy of DWF, deep convection was mostly enhanced during the rather dry periods as part of the TP, part of the RP and EMA supporting previous hypothesis that linked events of reinforced DWF to enhanced evaporation-precipitation balance (Cisneros et al., 2019). However, a perfect match between high $\delta^{18}O$ values and high UP10 is not always evident, since this connection in compromised by the uncertainties in the marine chronologies, its lower resolution and the speleothem hiatus during the MCA and LIAa.

The obtained record of Mallorca hydrology shares some features with hydrological reconstructions from Basa de la Mora and Estanya lakes (Fig. 7), in the north-eastern Iberian Peninsula (Morellón et al., 2009, 2011; Pérez-Sanz et al., 2013). Basa de la Mora Lake is located in the central Pyrenees at the modern transition between the Atlantic and Mediterranean climate regimes. The common features between Mallorca record and Basa de la Mora Lake, reinforce the Mediterranean influence in this site during the studied interval (Pérez-Sanz et al., 2013). Regarding to the salinity reconstruction from Estanya lake record, unfortunately the driest period represented by the Balearic record (RP) corresponds to a low resolution period in the lake record while the driest period detected in the Estanya lake record (MCA-LIAa) occurred during the hiatus in the Mallorca record, these circumstances prevent the establishment of solid comparisons between these two regions.

The only available paleoclimatic record in the Western Mediterranean region with comparable resolution and accurate

chronology is represented by a stalagmite composite record from north of Morocco (Ait Brahim et al., 2019). Curiously, when this is compared with our Mallorca record, they show a broadly opposite trend during the RP with extreme dry conditions in Mallorca when Morocco stalagmites indicate wetter conditions. In contrast, during the EMA and at the LIAb overall humidity patterns appear to be more homogeneous between the two regions (Fig. 7; Ait Brahim et al., 2017, 2018).

Last millennial precipitation changes in the Western Mediterranean are often associated with NAO dynamics (Wassenburg et al., 2016; Hernández et al., 2020; Moreno et al., 2012). Current observations in North Morocco support a negative correlation between rainfall amount and winter NAO index (Wassenburg et al., 2016). The last millennium $\delta^{18}O$ speleothem record from Grotte de Piste Cave (North Morocco) identifies the LIA by the dominance of light values interpreted as wet conditions associated to negative NAO values, an opposite situation than that detected for the MCA (Ait Brahim et al., 2018). The Mallorca composite $\delta^{18}O$ record only covers the last part of the LIA but also suggests relatively wet conditions that end with a relatively dry phase associated to more positive NAO values (Faust et al., 2016) (Fig. 7). Focusing on the older periods, most of the Mallorca dry periods correspond to positive NAO phases, in particular the second part of the RP and EMA, but this relation is less evident during the TP (Fig. 7). In spite of an overall congruent pattern with positive (negative) NAO and dry (humid) conditions in Mallorca, the correlation between our $\delta^{18}O$ record and the NAO is moderate ($r = 0.33$) using the Faust et al. (2016) NAO reconstruction, and comparable values or even lower are found with other available NAO reconstructions (Baker et al., 2015; Olsen et al., 2012; Trouet et al., 2009); (Table S5). This situation points out that other factors, different to NAO, also exerted a relevant role controlling the humidity over Mallorca during the last two millennia interpreted in base to the $\delta^{18}O$ composite record. A further interesting aspect of the parallel comparison of both Mallorca and Morocco speleothem records (Fig. 7) is the previously mentioned change in their relationship before and after the EMA. Although an accurate interpretation of this feature needs a more complete geographical coverage of comparable humidity records, it is interesting to note that previous studies in the Mediterranean have already identified evidences of changes in the potential relationship of different modes of climate variability such as NAO/EA, SCAN and EA/WR along the last two millennia (Roberts et al., 2012; Sánchez-López et al., 2016; Cisneros et al., 2019). The different location of the main pressure centres of the NAO but also its relationship with the other modes of climate variability could have distinctive response (non-stationary patterns) between the two compared regions (Wang et al., 2017; Comas-Bru and McDermott, 2014). Constraints of this apparent non-stationary pattern between the different modes of variability beyond the instrumental record are challenging and it requires of further research.

## 6. Conclusions

The first speleothem-based hydrological reconstruction from the central-western Mediterranean at sub-decadal resolution is presented here with a robust U-Th chronology from 653 yr BCE to 1880 yr CE. This consists of a $\delta^{18}O$ composite record of five speleothems from two Mallorca caves that cover the last 2.7 kyr with the exception of the MCA and earliest part of the LIA, which are represented by a hiatus in the sequence. In base to speleothem parameters such as $\delta^{13}C$ and trace element records (Mg/Ca, Sr/Ca and Ba/Ca) combined with mineralogical X-ray diffraction and stalagmite morphological analysis, and further complemented by information from a monitoring survey, the stalagmite composite $\delta^{18}O$ record is interpreted to reflect mostly PCP changes due to variable dripping rates controlled by regional hydrology. In particular, the geochemical signature of an almost five years sequence of calcite precipitates (2013–2018) shows a strong seasonal signal related to the annual cave ventilation cycle but, overprinting this, interannual variability reflects changes in annual average precipitation, with heaviest $\delta^{18}O$ values during the driest years.

The resulting composite $\delta^{18}O$ record indicates that generally wet conditions dominated for the Talaiotic Period (TP) and the early Roman Period (RP), the first half of the Early Middle Ages (EMA) and the second part of the Little Ice Age (LIAb), while dry conditions characterized the late RP, the late EMA. The comparison of this new hydrological record with a SST reconstruction from a nearby location, reveals that dry conditions occurred during both relatively cold but mostly warm intervals revealing a non-stationary complex climate relationship. An additional comparison with a proxy of deep convection in the Gulf of Lions, suggests a preferential occurrence of these events during drier conditions, although higher resolution and more accurate chronologies in the marine records would be required to establish tied connections between these marine and terrestrial archives.

The causes of the observed hydrological variability in the $\delta^{18}O$ record are explored by its comparison with a NAO reconstruction, indicating an overall consistency of dry periods in Mallorca during rather positive NAO phases. Nevertheless, correlation coefficients between the Mallorca speleothem record and NAO reconstructions are moderate-low indicating that NAO cannot explain the whole hydrological evolution in this region. When our new record is compared with another similar resolution stalagmite record from a cave in North Morocco, a contrasting pattern arises before and after the EMA, with opposite trends before in contrast to the parallel trends observed after the EMA. We propose that a complex non-stationary relationship between different modes of climate variability may explain this apparent difference on the regional hydrological patterns, which should be further explored by enhanced geographical coverage of comparable records.

## Declaration of competing interest

The authors declare that they have no known competing financial interests or personal relationships that could have appeared to influence the work reported in this paper.

## Acknowledgement

We thank financial support from ERC-Consolider Grant TIMED (683237); OPERA (CTM2013-48639-C2-1-R); PLIOKAR (CGL2013-48441-P); CHIMERA (CTM2016-75411-R); PLIOKAR-II (CGL2016-79246-P, AEI-FEDER, EU); SPYRIT (CGL2016-77479-R) and Generalitat de Catalunya, Grups de Recerca Consolidats (2017 SGR 315) to GRC Geociències Marines. We are grateful to M. Guart and A. Gallardo (Dept. de Dinàmica de la Terra i de l'Oceà, Universitat de Barcelona), J. Perona, T. Bullich, M. Aulet and À. San Martín for their collaboration in the laboratory tasks, and A. Pilares for his collaboration in the fieldwork. M. Cisneros benefited from a fellowship of the UB. IC thanks ICREA Academia programme from the Generalitat de Catalunya.

## Appendix A. Supplementary data

Supplementary data to this article can be found online at https://doi.org/10.1016/j.quascirev.2021.107137.

## References


Ait Brahim, Y., Cheng, H., Sifeddine, A., Wassenburg, J., Cruz, F.W., Khodri, M., shab, L., Pérez-Zanóni, N., Beraaouza, E.H., Apaésteguij, J., Guyotk, J.L., Jochumg, K.P., Bouchaoua, L., 2017. Speleothem records decadal to multidecadal hydroclimate variations in southwestern Morocco during the last millennium. Earth Planet Sci. Lett. 476, 1–10. https://doi.org/10.1016/j.epsl.2017.07.045.

Ait Brahim, Y., Wassenburg, J.A., Cruz, F.W., Sifeddine, A., Scholz, D., Bouchaou, L., Dassié, E.P., Jochum, K.P., Edwards, R.L., Cheng, H., 2018. Multi-decadal to centennial hydroclimate variability and linkage to solar forcing in the Western Mediterranean during the last 1000 years. Sci. Rep. 8, 17446. https://doi.org/10.1038/s41598-018-35498-x.

Ait Brahim, Y.A., Wassenburg, J.A., Sha, L., Cruz, F.W., Deininger, M., Sifeddine, A., Bouchaou, L., Spötl, C., Edwards, R.L., Cheng, H., 2019. North Atlantic ice-rafting, ocean and atmospheric circulation during the Holocene: insights from western Medterranean speleothems. Geophys. Res. Lett. 46, 7614–7623. https://doi.org/10.1029/2019GL082405.

Adloff, F., Somot, S., Sevault, F., Jordà, G., Aznar, R., Déqué, M., Herrmann, M., Marcos, M., Dubois, C., Padorno, E., Alvarez-Fanjul, E., Gomis, D., 2015. Mediterranean Sea response to climate change in an ensemble of twenty first century scenarios. Clim. Dynam. 45, 2775–2802. https://doi.org/10.1007/s00382-015-2507-3.

Anderson, T.F., Arthur, M.A., 1983. Stable isotopes of oxygen and carbon and their application to sedimentologic and paleoenvironmental problems. In: of SEPM, S.P. (Ed.), Stable Isotopes in Sedimentary Geology. https://doi.org/10.2110/scn.83.01.0000.

Baker, A., Hellstrom, J.C., Kelly, B.F.J., Mariethoz, G., Trouet, V., 2015. A composite annual-resolution stalagmite record of North Atlantic climate over the last three millennia. Sci. Rep. 5, 1–8.

Bar-Matthews, M., Ayalon, A., Gilmour, M., Matthews, A., Hawkesworth, C.J., 2003. Sea–land oxygen isotopic relationships from planktonic foraminifera and speleothems in the Eastern Mediterranean region and their implication for paleorainfall during interglacial intervals. Geochem. Cosmochim. Acta 67, 3181–3199.

Bartolomé, M., Moreno, A., Sancho, C., Stoll, H.M., Cacho, I., Spötl, C., Belmonte, A., Edwards, R.L., Cheng, H., Hellstrom, J.C., 2015. Hydrological change in southern Europe responding to increasing North Atlantic overturning during Greenland stadial 1. Proc. Natl. Acad. Sci. Unit. States Am. 112, 6568e6572. https://doi.org/10.1073/pnas.1503990112.

Bermejo, J., Mateu, T., López, B., Minguillón, R., Herráez, G., Villar, A., 2014. Cova de sa Balma des Quartó (Manacor, Mallorca). Endins: publicació d'espeleologia 59–64.

Bolòs, O. de, 1996. La vegetació de les Illes Balears. Institut d'Estudis Catalans, Barcelona, p. 269.

Boop, L.M., Onac, B.P., Wynn, J.G., Fornós, J.J., Rodríguez-Homar, M., Merino, A., 2014. Groundwater geochemistry observations in littoral caves of Mallorca (western Mediterranean): implications for deposition of phreatic overgrowths on speleothems. Int. J. Speleol. 43, 193–203.

Budsky, A., Scholz, D., Wassenburg, J.A., Mertz-Kraus, R., Spötl, C., Riechelmann, D.F., Gibert, L., Jochum, K.P., Andreae, M.O., 2019. Speleothem δ13C Record Suggests Enhanced Spring/summer Drought in South-Eastern Spain between 9.7 and 7.8 Ka–A Circum-Western Mediterranean Anomaly? Holocene, 0959683619838021. https://doi.org/10.1177/0959683619838021.

Carlson, P.E., Noronha, A.L., Banner, J.L., Jenson, J.W., Moore, M.W., Partin, J.W., Deininger, M., Breecker, D.O., Bautista, K.K., 2020. Constraining speleothem oxygen isotope disequilibrium driven by rapid $CO_2$ degassing and calcite precipitation: insights from monitoring and modelling. Geochem. Cosmochim. Acta 284, 222–238. https://doi.org/10.1016/j.gca.2020.06.012.

Cassou, C., Minvielle, M., Terray, L., Périgaud, C., 2010. A statistical dynamical scheme for reconstructing ocean forcing in the Atlantic. Part I: weather regimes as predictors for ocean surface variable. Clim. Dynam. 36 (1–2), 19–39.

Cheng, H., Edwards, L.R., Chou Shen, C., Polyak, V.J., Asmerom, Y., Woodhead, J., Hellstrom, J., Wang, Y., Kong, X., Spötl, C., Wang, X., Calvin Alexander, J.R., 2013. Improvements in $^{230}$Th dating, $^{230}$Th and $^{234}$U half-life values, and U-Th isotopic measurements by multi-collector inductively coupled plasma mass spectrometry. Earth Planet Sci. Lett. 371-372, 82–91.

Cheng, H., Sinha, A., Verheyden, S., Nader, F.H., Li, X.L., Zhang, P.Z., Yin, J.J., Yi, L., Peng, Y.B., Rao, Z.G., Ning, Y.F., Edwards, R.L., 2015. The climate variability in northern levant over the past 20,000 years: climate variability in northern levant. Geophys. Res. Lett. 42, 8641–8650. https://doi.org/10.1002/2015GL065397.

Cisneros, M., Cacho, I., Frigola, J., Canals, M., Masqué, P., Martrat, B., Casado, M., Grimalt, J.O., Pena, L.D., Margaritelli, G., Lirer, F., 2016. Sea surface temperature variability in the central-western Mediterranean Sea during the last 2700 years: a multi-proxy and multi-record approach. Clim. Past 12, 849–869. https://doi.org/10.5194/cp-12-849-2016.

Cisneros, M., Cacho, I., Frigola, J., Sanchez-Vidal, A., Pedrosa-Pàmies, R., Rumín-Caparrós and, A., Canals, M., 2019. Deep-water formation variability in the north-western Mediterranean Sea during the last 2500 yr: a proxy validation with present-day data. Global Planet. Change 177, 56–68. https://doi.org/10.1016/j.gloplacha.2019.03.012.

Comas-Bru, L., McDermott, F., 2014. Impacts of the EA and SCA patterns on the European twentieth century NAO-winter climate relationship: impacts of EA and SCA patterns on NAO-winter climate relationship. Q. J. R. Meteorol. Soc. 140, 354–363. https://doi.org/10.1002/qj.2158.

Craig, H., 1965. The measurement of oxygen isotope paleotemperatures. In: Tongiorgi, E. (Ed.), Stable Isotopes in Oceanographic Studies and Paleotemperatures, Consiglio Nazionale delle Ricerche, Laboratorio di Geologia Nucleare, pp. 1–24.

Dumitru, O.A., Onac, B.P., Fornós, J.J., Cosma, C., Ginés, A., Ginés, J., Merino, A., 2015. Radon survey in caves from Mallorca island, Spain. STOTEN 526, 196–203.

Dumitru, O.A., Forray, F.L., Fornós, J.J., Ersek, V., Onac, B.P., 2017. Water isotopic variability in Mallorca: a path to understanding past changes in hydroclimate. Hydrol. Process. 31, 104–116. https://doi.org/10.1002/hyp.10978.

Dumitru, O.A., Onac, B.P., Polyak, V.J., Wynn, J.G., Asmeron, Y., Fornós, J.J., 2018. Climate variability in the western Mediterranean between 121 and 67 ka derived from a Mallorcan speleothem record. Palaeogeogr. Palaeoclimatol. Palaeoecol. 506, 128–138. https://doi.org/10.1016/j.palaeo.2018.06.028.

Dumitru, O.A., Austermann, J., Polyak, V.J., Fornós, J.J., Asmerom, Y., Ginés, J., Ginés, A., Onac, B.P., 2019. Constraints on global mean sea level during Piocene warmth. Nature. https://doi.org/10.1038/s41586-019-1543-2.

Edwards, R.L., Chen, J.H., Wasserburg, G.J., 1987. $^{238}$U-234U-230Th-232Th systematics and the precise measurement of time over the past 500,000 years. Earth Planet Sci. Lett. 81, 175–192.

Enseñat, J.J., Gràcia, F., Ginard, A., Mascaró, G., Santandreu, G., Fernández, J.F., Trias, M., Pérez, J., Bover, P., Cirer, A., Pla, V., Lázaro, J.C., Vicens, D., Ansaldi, D., Bascuñana, F.X., Clamor, B., Lozano, A., Perelló, M.À., Gual, M.À., Vives, M.À., Gaviño, B., Gamund, P., Bonnin, M., Granell, À., Betton, N., Franglen, N., Bornemann, D., 2019. Nou plànol topogràfic de les coves del drac (Manacor, Mallorca). Papers de La Societat Espeleològica Balear 1, 65–76. http://socespbal.blogspot.com/p/papers1.html.

Fairchild, I.J., Borsato, A., Tooth, A.F., Frisia, S., Hawkesworth, C.J., Huang, Y.M., McDermott, F., Spiro, B., 2000. Controls on trace element (Sr-Mg) compositions of carbonate cave waters: implications for speleothem climatic records. Chem. Geol. 166, 255–269.

Fairchild, I.J., Treble, P.C., 2009. Trace element in speleothems as recorders of environmental change. Quat. Sci. Rev. 28, 449–468.

Faust, J.C., Fabian, K., Milzer, G., Giraudeau, J., Knies, J., 2016. Norwegian fjord sediments reveal NAO related winter temperature and precipitation changes of the past 2800 years. Earth Planet Sci. Lett. 435, 84–93. https://doi.org/10.1016/j.epsl.2015.12.003.

Feldmann, R.M., Chapman, R.E., Hannibal, J.T., 1989. Paleotechniques. The Paleontological Society, Special Publication, p. 4.

Fohlmeister, J., 2012. A statistical approach to construct composite climate records of dated archives. Quat. Geochronol. 14, 48–56. https://doi.org/10.1016/j.quageo.2012.06.007.

Frisia, S., Borsato, A., Preto, N., McDermott, F., 2003. Late Holocene annual growth in three Alpine stalagmites records the influence of solar activity and the North Atlantic Oscillation on winter climate. Earth Planet. Sci. Lett. 216, 411–424.

Frisia, S., Borsato, A., Spötl, C., Villa, I.M., Cucchi, F., 2005. Climate variability in the SE Alps of Italy over the past 17 000 years reconstructed from a stalagmite record. Boreas 34, 445–455. https://doi.org/10.1080/03009480500231336.

Frisia, S., Borsato, A., Mangini, A., Spötl, C., Madonia, G., Sauro, U., 2006. Holocene climate variability in sicily from a discontinuous stalagmite record and the Mesolithic to neolithic transition. Quat. Res. 66, 388–400. https://doi.org/10.1016/j.yqres.2006.05.003.

Garcia, J., Delgado, X., Ferrreres, J., 1986. Recull de cavitats de l'illa de Mallorca.

Ginés, J., Ginés, A., 1976. Ses Coves del Pirata. Endins 3, 41–45.

Ginés, J., Ginés, A., 2011. Les coves turístiques de les Illes Balears: antecedents i estat de la qüestió, Endins 35. Mon. Soc. Hist. Nat. Balears 17, 333–344.

Ginés, J., Fornós, J., Ginés, A., Merino, A., Gràcia, F., 2014. Geologic constraints and speleogenesis of Cova des Pas de Vallgornera, a complex coastal cave from Mallorca Island (Western Mediterranean). Int. J. Speleol. 43 (2), 105–124.

Giorgi, F., 2006. Climate change hot-spots. Geophys. Res. Lett. 33. https://doi.org/10.1029/2006GL025734.

Hernández, A., Sánchez-López, G., Pla-Ribes, S., Comas-Bru, L., Parnell, A., Cahill, N., Geyer, A., Trigo, R.M., Giralt, S., 2020. A 2,000-year Bayesian NAO reconstruction from the iberian Peninsula. Nat. Sci. Rep. https://doi.org/10.1038/s41598-020-71372-5.

Hodge, E.J., 2004. Palaeoclimate of the Western Mediterranean Region: Results from Speleothems. Ph.D. Thesis. University of Bristol, Bristol (Unpublished).

Hodge, E.J., Richards, D.A., Smart, P.L., Ginés, A., Mattey, D.P., 2008. Sub-millennial climate shifts in the western Mediterranean during the last glacial period recorded in a speleothem from Mallorca, Spain. J. Quat. Sci. 23, 713–718. https://doi.org/10.1002/jqs.1198.

Homar, V., Ramis, C., Romero, R., Alonso, S., 2010. Recent trends in temperature and precipitation over the Balearic Islands (Spain). Climatic Change 98, 199–211. https://doi.org/10.1007/s10584-009-9664-5.

Hurrell, J.W., 1995. Decadal trends in the north atlantic oscillation: regional temperatures and precipitation. Science 269, 676–679. https://doi.org/10.1126/science.269.5224.676.

An overview of the north atlantic oscillation. In: Hurrell, J.W., Kushnir, Y., Visbeck, M., Ottersen, G. (Eds.), 2003. The North Atlantic Oscillation, Geophysical Monograph Series, vol. 134. American Geophysical Union, Washington, DC. https://doi.org/10.1029/134GM01.

Josey, S.A., Somot, S., Tsimplis, M., 2011. Impacts of atmospheric modes of variability on Mediterranean Sea surface heat exchange. J. Geophys. Res. 116. https://doi.org/10.1029/2010JC006685.

Kaufmann, G., Dreybrodt, W., 2004. Stalagmite growth and palaeo-climate: an

inverse approach. Earth Planet Sci. Lett. 224, 529–545. https://doi.org/10.1016/j.epsl.2004.05.020.
Lechleitner, F.A., Amirnezhad-Mozhdehi, S., Columbu, A., Comas-Bru, L., Labuhn, I., Pérez-Mejías, C., Rehfeld, K., 2018. The potential of speleothems fromWestern Europe as recorders of regional climate: a critical assessment of the SISAL database. Quaternary 1, 30. https://doi.org/10.3390/quat1030030.
Lionello, P., Sanna, A., 2005. Mediterranean wave climate variability and its links with NAO and Indian Monsoon. Clim. Dynam. 25, 611–623. https://doi.org/10.1007/s00382-005-0025-4.
Lionello, P., Malanotte-Rizzoli, P., Boscolo, R., 2006. Mediterranean Climate Variability. Elsevier.
Mangini, A., Spötl, C., Verdes, P., 2005. Reconstruction of temperature in the Central Alps during the past 2000 yr from a $\delta^{18}O$ stalagmite record. Earth Planet Sci. Lett. 235, 741–751.
Margaritelli, G., Cacho, I., Català, A., Barra, M., Bellucci, L.G., Lubritto, C., Rettori, R., Lirer, F., 2020. Persistent warm Mediterranean surface waters during the Roman period. Sci. Rep. 10. https://doi.org/10.1038/s41598-020-67281-2.
Mariotti, A., 2011. Decadal climate variability and change in the Mediterranean Region. In: Sci. Technol. Infus. Clim. Bull., Climate Test Bed Joint Seminar Series. US National Oceanic and Atmospheric Administration, Maryland, pp. 1–5.
Martel, E.A., 1903. "Les cavernes de Majorque". Spelunca 32 (5) (Paris).
Martín-Chivelet, J., Muñoz-García, M.B., Edwards, R.L., Turrero, M.J., Ortega, A.I., 2011. Land surface temperature changes in Northern Iberia since 4000 yr BP, based on $\delta^{13}C$ of speleothems. Global Planet. Change 77, 1–12. https://doi.org/10.1016/j.gloplacha.2011.02.002.
Martín-Chivelet, J., Muñoz-García, M.B., Cruz, J.A., Ortega, A.I., Turrero, M.J., 2017. Speleothem Architectural Analysis: integrated approach for stalagmite-based paleoclimate research. Sediment. Geol. 353, 28–45. https://doi.org/10.1016/j.sedgeo.2017.03.003.
McMillan, E.A., Fairchild, I.J., Frisia, S., Borsato, A., McDermott, F., 2005. Annual trace element cycles in calcite-aragonite speleothems: evidence of drought in the western Mediterranean 1200-1100 yr BP. J. Quat. Sci. 20, 423–433.
Mickler, P.J., Stern, L.A., Banner, J.L., 2006. Large kinetic isotope effects in modern speleothems. Geol. Soc. Am. Bull. 118, 65–81. https://doi.org/10.1130/B25698.1.
Mischel, S.A., Scholz, D., Spötl, C., Jochum, K.P., Scröder-Ritzrau, Fiedler, S., 2016. Holocene climate variability in Central Germany and a potential link to the polar North Atlantic: a replicated record from three coeval speleothems. Holocene 1–17. https://doi.org/10.1177/0959683616670246.
Morellón, M., Valero-Garcés, B., Vegas-Vilarrúbia, T., González-Sampériz, P., Romero, Ó., Delgado-Huertas, A., Mata, P., Moreno, A., Rico, M., Corella, J.P., 2009. Lateglacial and Holocene palaeohydrology in the western Mediterranean region: the lake Estanya record (NE Spain). Quat. Sci. Rev. 28, 2582–2599. https://doi.org/10.1016/j.quascirev.2009.05.014.
Morellón, M., Valero-Garcés, B., González-Sampériz, P., Vegas-Vilarrúbia, T., Rubio, E., Rieradevall, M., Delgado-Huertas, A., Mata, P., Romero, Ó., Moreno, A., Engstrom, D.R., López-Vicente, M., Navas, A., Soto, J., 2011. Climate changes and human activities recorded in the sediments of lake Estanya (NE Spain) during the Medieval warm period and little Ice age. J. Paleolimnol. 46, 423–452. https://doi.org/10.1007/s10933-009-9346-3.
Moreno, A., Stoll, H., Jiménez-Sánchez, M., Cacho, I., Valero-Garcés, B., Ito, E., Edwards, R.L., 2010. A speleothem record of glacial (25-11.6 kyr BP) rapid climatic changes from northern Iberian Peninsula. Global Planet. Change 71, 218–231. https://doi.org/10.1016/j.gloplacha.2009.10.002.
Moreno, A., Pérez, A., Frigola, J., Nieto-Moreno, V., Rodrigo-Gámiz, M., Martrat, B., González-Sampériz, P., Morellón, M., Martín-Puertas, C., Pablo, J., Belmonte, Á., Sancho, C., Cacho, I., Herrera, G., Canals, M., Grimalt, J.O., Jiménez-Espejo, F., Martínez-Ruiz, F., Vegas-Vilarrúbia, T., Valero-Garcés, B.L., 2012. The Medieval climate anomaly in the iberian Peninsula reconstructed from marine and lake records. Quat. Sci. Rev. 43, 16–32. https://doi.org/10.1016/j.quascirev.2012.04.007.
Moreno, A., Iglesias, M., Azorin-Molina, C., Pérez-Mejías, C., Bartolomé, M., Sancho, C., Stoll, H., Cacho, I., Frigola, J., Osácar, C., Muñoz, A., Delgado-Huertas, A., Blade, I., Vimeux, F., 2021. Spatial variability of northern Iberian rainfall stable isotope values: investigating climatic controls on daily and monthly timescales. Atmos. Chem. Phys. Discuss. 1–34. https://doi.org/10.5194/acp-2020-861.
Mühlinghaus, C., Scholz, D., Mangini, A., 2009. Modelling fractionation of stable isotopes in stalagmites. Geochem. Cosmochim. Acta. 73 (24), 7275–7289. https://doi.org/10.1016/j.gca.2009.09.010.
Nagra, G., Treble, P.C., Andersen, M.S., Bajo, P., Hellstrom, J., Baker, A., 2017. Dating stalagmites in Mediterranean climates using annual trace element cycles. Sci. Rep. 7, 621. https://doi.org/10.1038/s41598-017-00474-4.
Neukom, R., Steiger, N., Gómez-Navarro, J.J., Wang, J., Werner, J.P., 2019. No evidence for globally coherent warm and cold periods over the pre-industrial Common Era. Nat. Lett. Res. 571, 550–554. https://doi.org/10.1038/s41586-019-1401-2.
Olsen, J., Anderson, N.J., Knudsen, M.F., 2012. Variability of the north atlantic oscillation over the past 5200 years. Nat. Geosci. 5, 808–812. https://doi.org/10.1038/ngeo1589.
Parnell, A.C., Haslett, J., Allen, J.R.M., Buck, C.E., Huntley, B., 2008. A flexible approach to assessing synchroneity of past events using Bayesian reconstructions of sedimentation history. Quat. Sci. Rev. 27, 1872–1885. https://doi.org/10.1016/j.quascirev.2008.07.009.
Pérez-Mejías, C., Moreno, A., Sancho, C., Bartolomé, M., Stoll, H., Cacho, I., Cheng, H., Edwards, R.L., 2017. Abrupt climate changes during termination III in southern Europe. Proc. Natl. Acad. Sci. Unit. States Am. 114, 10047–10052.
Pérez-Mejías, C., Moreno, A., Sancho, C., Martín-García, R., Spötl, C., Cacho, I., Cheng, H., Edwards, R.L., 2019. Orbital-to-millennial scale climate variability during marine isotope stages 5 to 3 in northeast iberia. Quat. Sci. Rev. 224. https://doi.org/10.1016/j.quascirev.2019.105946.
Pérez-Sanz, A., González-Sampériz, P., Moreno, A., Valero-Garcés, B., Gil-Romera, G., Rieradevall, M., Tarrats, P., Lasheras-Álvarez, L., Morellón, M., Belmonte, A., Sancho, C., Sevilla-Callejo, M., Navas, A., 2013. Holocene climate variability, vegetation dynamics and fire regime in the central Pyrenees: the Basa de la Mora sequence (NE Spain). Quat. Sci. Rev. 73, 149–169. https://doi.org/10.1016/j.quascirev.2013.05.010.
Polyak, V.P., Onac, B.P., Fornós, J.J., Hay, C., Asmeron, Y., Dorale, J.A., Ginés, J., Tuccimei, P., Ginés, A., 2018. A highly resolved record of relative sea level in the western Mediterranean Sea during the last interglacial period. Nat. Geosci. 11, 860–864. https://doi.org/10.1038/s41561-018-0222-5.
Railsback, L.B., Liang, F., Vidal Romaní, J.R., Grandal d'Anglade, A., Vaqueiro Rodríguez, M., Santos Fidalgo, L., Fernández Mosquera, D., Cheng, H., Edwards, R.L., 2011. Petrographic and isotopic evidence for Holocene long-term climate change and shorter-term environmental shifts from a stalagmite from the Serra do Courel of northwestern Spain, and implications for climatic history across Europe and the Mediterranean. Palaeogeogr. Palaeoclimatol. Palaeoecol. 305, 172–184. https://doi.org/10.1016/j.palaeo.2011.02.030.
Riechelman, D.F.C., Deiniger, M., Scholz, D., Riechelman, S., Schröder-Ritzrau, A., Spötl, C., Richter, D.K., Mangini, A., Immenhauser, A., 2013. Disequilibrium carbon and oxygen isotope fractionation in recent cave calcite: comparison of cave precipitates and model data. Geochem. et Cosmochem. Acta 103, 232–244. https://doi.org/10.1016/j.gca.2012.11.002.
Roberts, N., Moreno, A., Valero-Garcés, B.L., Corella, J.P., Jones, M., Allcock, S., Woodbridge, J., Morellón, M., Luterbacher, J., Xoplaki, E., Türkeş, M., 2012. Palaeolimnological evidence for an east–west climate see-saw in the Mediterranean since AD 900. Global Planet. Change 84–85, 23–34. https://doi.org/10.1016/j.gloplacha.2011.11.002.
Roesch, C., Rehfeld, K., 2019. Automatising age-depth modelling for hundreds of speleothems. In: Conference paper at 9th International Workshop on Climate Informatics.
Sánchez-López, G., Hernández, A., Pla-Rabes, S., Trigo, R.M., Toro, M., Granados, I., Sáez, A., Masqué, P., Pueyo, J.J., Rubio-Inglés, M.J., Giralt, S., 2016. Climate reconstruction for the last two millennia in central iberia: the role of East Atlantic (EA), North Atlantic oscillation (NAO) and their interplay over the iberian Peninsula. Quat. Sci. Rev. 149, 135–150. https://doi.org/10.1016/j.quascirev.2016.07.021.
Sinclair, D.J., Allard, G., Williams, B., Ross, S., Risk, M.J., 2011. Reproducibility of trace element profiles in a specimen of the deep-water bamboo coral keratoisis sp. Geochem. Cosmochim. Acta 75 (18), 5101–5121.
Sinclair, D.J., Banner, J.L., Taylor, F.W., Partin, J., Jenson, J., Mylroie, J., Goddard, E., Quinn, T., Jocson, J., Miklavič, B., 2012. Magnesium and strontium systematics in tropical speleothems from the Western Pacific. Chem. Geol. 294–295, 1–17.
Stoll, H.M., Muller, W., Prieto, M., 2012. I-STAL, a model for interpretation of Mg/Ca, Sr/Ca and Ba/Ca variations in speleothems and its forward and inverse application on seasonal to millennial scales. G-cubed 13, 27.
Torner, J., Cacho, I., Moreno, A., Sierro, F.J., Martrat, B., Rodriguez-Lazaro, J., Frigola, J., Arnau, P., Belmonte, A., Hellstrom, J., Cheng, H., Edwards, R.L., Stoll, H., 2019. Ocean-atmosphere interconnections from the last interglacial to the early glacial: an integration of marine and cave records in the Iberian region. Quat. Sci. Rev. 226. https://doi.org/10.1016/j.quascirev.2019.106037.
Treble, P., Shelley, J.M.G., Chappell, J., 2003. Comparison of high-resolution subannual records of trace elements in a modern (1911–1992) speleothem with instrumental climate data from southwest Australia. Earth Planet Sci. Lett. 216, 141–153.
Trigo, I.F., Bigg, G.R., Davies, T.D., 2002. Climatology of cyclogenesis mechanisms in the Mediterranean. Mon. Weather Rev. 130, 549–569.
Trouet, V., Esper, J., Graham, N.E., Baker, A., Scourse, J.D., Frank, D.C., 2009. Persistent positive North Atlantic oscillation mode dominated the Medieval climate anomaly. Science 324, 78–80. https://doi.org/10.1126/science.1166349.
Vesica, P.L., Tuccimei, P., Turi, B., Fornós, J.J., Ginés, A., Ginés, J., 2001. Late Pleistocene Paleoclimates and sea-level change in the Mediterranean as inferred from stable isotope and U-series studies of overgrowths on speleothems, Mallorca, Spain. Quat. Sci. Rev. 19, 865–879.
Wang, J., Yang, B., Ljungqvist, F.C., Luterbacher, J., Osborn, T.J., Briffa, K.R., Zorita, E., 2017. Internal and external forcing of multidecadal Atlantic climate variability over the past 1,200 years. Nat. Geosci. 10, 512–518. https://doi.org/10.1038/NGEO2962. July 2017.
Wassenburg, J.A., Immenhauser, A., Richter, D.K., Niedermayr, A., Riechelmann, S., 2013. Moroccan speleothem and tree ring records suggest a variable positive state of the North Atlantic Oscillation during the Medieval Warm Period. Earth Planet. Sci. Lett. 375, 291–302. https://doi.org/10.1016/j.epsl.2013.05.048.
Wassenburg, J.A., Dietrich, S., Fietzke, J., Fohlmeister, J., Jochum, K.P., Scholz, D., Richter, D.K., Sabaoui, A., Spötl, C., Lohman, G., Andreae, M.O., Immenhauser, A., 2016. Reorganization of the north atlantic oscillation during early Holocene deglaciation. Nat. Geosci. https://doi.org/10.1038/ngeo2767.
Wassenburg, J.A., Riechelman, S., Schöder-Ritzrau, A., Riechelman, D.F.C., Richter, D.K., Immenhauser, A., Terente, M., Constantin, S., Hachenberg, A., Hansen, M., Scholz, D., 2020. Calcite Mg and Sr partition coefficients in cave environments: implications for interpreting prior calcite precipitation in speleothems. Geochem. et Comochim. Act. 269, 581–596.